Optimized planar Penning traps for quantum-information studies

J. Goldman and G. Gabrielse*

Department of Physics, Harvard University, Cambridge, Massachusetts 02138, USA
(Received 4 February 2010; published 24 May 2010)

A one-electron qubit would offer a new option for quantum information science, including the possibility of extremely long coherence times. One-quantum cyclotron transitions and spin flips have been observed for a single electron in a cylindrical Penning trap. However, an electron suspended in a planar Penning trap is a more promising building block for the array of coupled qubits needed for quantum information studies. The optimized design configurations identified here promise to make it possible to realize the elusive goal of one trapped electron in a planar Penning trap—a substantial step toward a one-electron qubit.

PACS number(s): 03.67.−a, 37.10.Ty

I. INTRODUCTION

Quantum jumps [1] have been observed between the lowest cyclotron and spin states of an electron suspended in the magnetic field of a cylindrical Penning trap (Fig. 1). These observations made possible the most precise measurements of the electron magnetic moment and the fine-structure constant [2]. The one-electron observations also triggered intriguing studies on using one-electron qubits as building blocks for quantum information processing [3–14]. The possibility of a very long coherence time is very attractive.

A new trap design is needed to realize one-electron qubits for quantum information studies. Although a single electron in a single trap is the focus of this work, a scalable array of coupled one-electron qubits is the long-term goal. Impressive progress has been made in the microfabrication of three-dimensional trap arrays [15], but it is still beyond these or more traditional methods to fabricate a large array of small cylindrical traps with the properties needed to observe one-quantum transitions with one electron. A scalable array of small traps seems more feasible with traps whose electrodes are entirely in a plane since these could be fabricated on a chip using variations on more standard microfabrication methods [14]. The chip could include electrical couplings between the traps, and could even include some detection electronics. Secondary advantages of a planar trap would be an open structure that makes it easier to introduce microwaves (to modify or entangle electron spin states) and possibly to load electrons.

One possible planar Penning trap geometry (Fig. 2) is a round center electrode with concentric rings [10]. Electrons were stored and observed in such a trap, first in Mainz [11,12] and then in Ulm [13]. The objective of the latter experiment was to duplicate in a planar trap the observations of the one-quantum transitions of a single electron in a cylindrical Penning trap (Fig. 1). The final experimental report [13] is not encouraging. It concludes that the "lack of mirror symmetry" makes it "impossible to create a genuinely harmonic potential" and that it is thus "impossible" to detect a single electron within a planar Penning trap. Whether the situation changes with much smaller planar traps is being considered [14].

We reach a more optimistic conclusion in this work, though the pessimism may be appropriate for the trap designs used so far. The key to a successful planar trap for one electron is a design that minimizes amplitude-dependent frequency shifts of the observed oscillation frequency. This report focuses upon calculating the relationship of such shifts to the electrode geometry and applied potentials. (Appendix A corrects an earlier calculation [10] of the crucial amplitude-dependent frequency shifts needed to characterize and optimize planar traps.) We identify optimized planar Penning trap geometries and potentials that produce amplitude-dependent frequency shifts that are orders of magnitude smaller than for previous planar trap designs.

A high measurement precision with a single trapped particle is part of what will be required to observe a spin flip and realize a one-electron qubit. Several of the most accurate measurements in physics illustrate the feasibility of attaining the needed precision when a trap design that is optimized for the particular high-precision application is used. The cylindrical Penning trap of Fig. 1(c) [16] was designed so that its electrodes form a microwave cavity that inhibits spontaneous emission. This trap design enabled the observation of one-quantum transitions, which made possible the most accurate measurements of the electron magnetic moment and the fine-structure constant [2]. An orthogonalized hyperbolic trap [17,18] was designed to allow a trapping potential to be optimized without changing the trap depth. The most precise mass spectroscopy (e.g., [19]) was carried out in such a trap with a single ion (or two). An open-access Penning trap [20] was designed to allow antiprotons from an accelerator facility to enter the trap. The most accurate comparison of q/m for an antiproton and proton [21] was carried out with a single antiproton and a single H$^-$ ion in such a trap, as were the most accurate one-ion measurements of bound electron g values [22,23] and the most precise proton-to-electron mass ratio [24]. Inspired by these examples, this study of planar Penning traps for one-electron applications is carried out in the hope that a similar rigorous design approach will indicate the best route to observing one electron in a planar trap.

Optimized geometries and biasing schemes identified here for planar Penning traps promise to reduce the amplitude dependence of the observed frequency by many orders of magnitude. This reduction makes it much more likely that one electron can be observed in a planar Penning trap—an
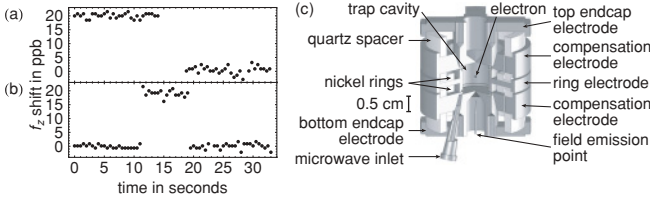
---

*gabrielse@physics.harvard.edu

FIG. 1. (a) Quantum nondemolition (QND) observation of a spin flip of one trapped electron. (b) QND observation of a one-quantum cyclotron transition for one electron. (c) Cylindrical Penning trap within which the electron is suspended.

important first step toward realizing a one-electron qubit. Two related trap configurations, a covered planar trap and a mirror-image trap, offer improved shielding, new detection options, and easier trap loading. It remains, of course, to demonstrate experimentally that the optimized planar trap designs proposed will approach the performance of the cylindrical Penning trap in which one-quantum transitions and spin flips of a single electron were observed.

II. OUTLINE

Section III describes the potential and potential expansions for a planar Penning trap. Section IV relates the amplitude dependence of the particle's axial oscillation frequency to the potential expanded around the equilibrium location of the trapped particle. The axial oscillation of a trapped particle must be detected to tell that a single particle is in the trap. Small shifts in this frequency will reveal spin flips and one-quantum cyclotron transitions.
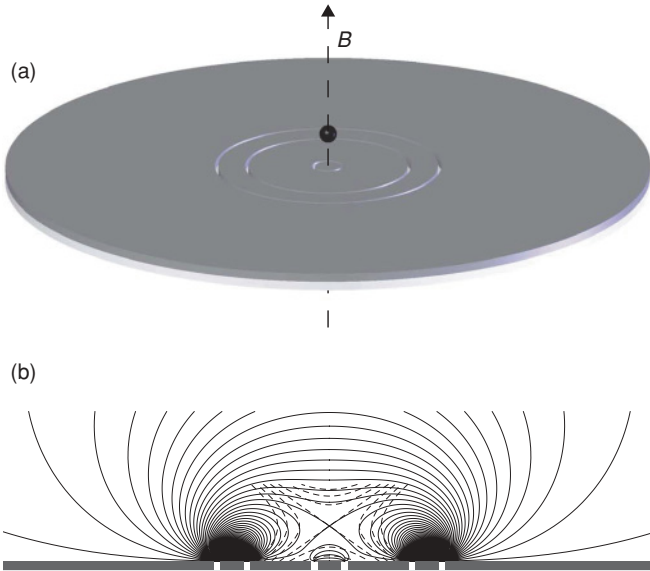

FIG. 2. (a) Three-gap planar trap with a trapped particle suspended above an electrode plane that extends to infinity. (b) Side view of trap electrodes and equipotentials spaced by V_0, with the infinitesimal gaps between the electrodes widened to make them visible. The equipotentials extend into the gaps between electrodes. The dashed equipotentials of an ideal quadrupole are superimposed near the trap center.

Two-gap traps (with two biased electrodes surrounded by a ground plane) are shown in Sec. V to be inadequate for the observation and the manipulation of a single electron. The considerable promise of three-gap traps (with three biased electrodes surrounded by a ground plane) is the subject of Sec. VI. Optimized planar trap configurations that make the particle's oscillation frequency essentially independent of oscillation amplitude are identified and discussed, along with the detection and damping of the particle's motion.

Section VII estimates the size of the unavoidable deviations between ideal planar Penning traps and the actual laboratory traps. Real traps have gaps between electrodes, finite boundary conditions, and imperfections in the trap dimensions, all of which must be compensated by modifying the voltages applied to the trap electrodes.

A covered planar trap (a two-gap planar trap covered by a parallel conducting plane) is proposed in Sec. VIII A as a scalable way to make planar chip traps less sensitive to nearby apparatus. An electron suspended midway between a mirror-image pair of planar electrodes is shown in Sec. VIII B to be in a potential with much the same properties as is experienced by an electron centered in a cylindrical Penning trap. For an electron initially loaded and observed in an "orthogonalized" mirror-image trap, we illustrate in Sec. VIII C the possibility to adiabatically change the applied trapping potentials to move the electron into a covered planar Penning trap that is optimized.

The damping and detection of a particle in planar traps, covered planar traps, and mirror-image traps are considered in Sec. IX. The optimization of damping and detection is discussed, as are unique detection opportunities available with a covered planar trap.

A conclusion in Sec. X is followed by three appendices. Appendix A corrects an earlier calculation of amplitude-dependent frequency shifts in a planar trap. Appendices B and C use the calculations of this work to analyze the properties of planar traps built at Mainz and Ulm.

III. PLANAR PENNING TRAPS

A. The ideal to be approximated

An ideal Penning trap, which we seek to approximate, starts with a spatially uniform magnetic field,

$$\mathbf{B} = B\hat{\mathbf{z}}. \qquad (1)$$

Superimposed is an electrostatic quadrupole potential, $V_2(\rho, z)$ in cylindrical coordinates, that is a harmonic oscillator potential on the $\rho = 0$ axis,

$$V_2(0, z) = \frac{1}{2} V_0 \left(\frac{z - z_0}{\rho_1} \right)^2, \qquad (2)$$

where ρ_1 sets the size scale for the trap and V_0 sets the potential scale.

A particle of charge q and mass m on axis then oscillates at an axial angular frequency

$$\omega_z = \sqrt{\frac{q}{m} \frac{V_0}{\rho_1^2}}, \qquad (3)$$

about the potential minimum at z_0. The potential will trap a particle only if $q V_0 > 0$.

The axial oscillation frequency ω_z is the key observable for possible quantum information studies. The one-quantum cyclotron and spin-flip transitions that have been observed [e.g., Figs. 1(a) and (b)] were detected using the small shifts in ω_z caused by a quantum nondemolition (QND) coupling of the cyclotron and spin energies to ω_z.

For potentials that can be expressed on an axis of symmetry as a power series in $z - z_0$ [e.g., Eq. (2)], the general solution to Laplace's equation near the point $(0, z_0)$ is related to the axial solution by the substitution,

$$(z - z_0)^k \to [\rho^2 + (z - z_0)^2]^{k/2} P_k[\cos(\theta)], \qquad (4)$$

where $\cos(\theta) = (z - z_0)/\sqrt{\rho^2 + (z - z_0)^2}$ and P_k is a Legendre polynomial. We will focus upon axial potentials throughout this work since this procedure can be used to obtain the general potential in the neighborhood of any axial position when this is needed.

Applied to the harmonic axial potential of an ideal Penning trap,

$$V_2(\rho, z) = \frac{V_0}{2} \frac{\rho^2 + (z - z_0)^2}{\rho_1^2} P_2[\cos(\theta)]. \qquad (5)$$

This quadrupole potential for an ideal Penning trap extends through all space.

B. Electrodes in a plane

A planar Penning trap (Figs. 2 and 3) starts with a spatially uniform magnetic field as in Eq. (1). An electrostatic potential is produced by biasing N ring electrodes in a plane perpendicular to the symmetry axis of the electrodes $\hat{\mathbf{z}}$. An electrode with an outer radius ρ_i is biased to a potential V_i, as illustrated in Fig. 3. Without loss of generality, the potential beyond the rings $\rho > \rho_N$ is taken to be the zero of potential $V_{N+1} = 0$. The N gaps between biased electrodes are taken initially to be infinitesimal, but this condition is relaxed in Sec. VII A.

Two remaining boundary conditions,

$$V(\rho, z \to \infty) = 0, \qquad (6a)$$
$$V(\rho \to \infty, z) = 0, \qquad (6b)$$

will be assumed to derive the potential for $z \geqslant 0$. It is not always possible in real apparatus to keep all metal far enough away from the trap electrodes so that these boundary conditions are accurately satisfied. We consider the case of finite boundary conditions in Sec. VII C.

Throughout this work we will illustrate the basic features and challenges of a planar Penning trap using a three-gap ($N = 3$) sample trap with dimensions

$$\{\rho_i\} = \{1, 5.5, 7.5426\}\rho_1, \qquad (7)$$

for reasons discussed in Sec. VI. Figure 3 shows this relative geometry (to scale).

C. Scaling distances and potentials

It is natural and often useful to scale distances in terms of the radius of the inner electrode ρ_1. We will do so, using the notation $\tilde{z} = z/\rho_1$ and $\tilde{\rho} = \rho/\rho_1$. The relative geometry of a
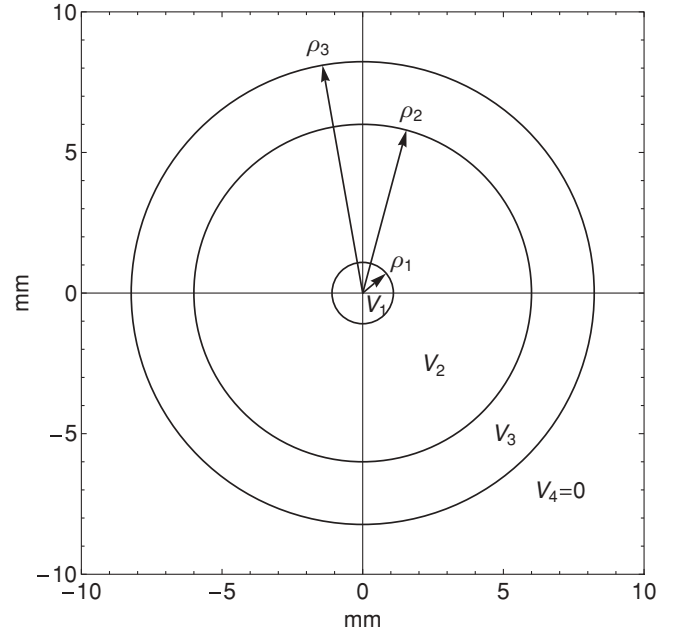

FIG. 3. Rings of a planar Penning trap. The relative geometry of the electrodes is that of the sample trap used to illustrate the general features of planar traps. Infinitesimal gaps between electrodes are assumed until Sec. VII A.

planar Penning trap is then given by the set of dimensions $\{\tilde{\rho}_i\} = \{1, \tilde{\rho}_2, \tilde{\rho}_3, \ldots\}$, for example.

It is natural and convenient to scale the trap potential V, along with the voltages V_i applied to trap electrodes, in terms of a voltage scale, V_0, to be determined. We will then use scaled applied potentials, $\tilde{V}_i = V_i/V_0$, and a scaled trap potential $\tilde{V} = V/V_0$.

D. Exact superposition

The potential produced by a planar Penning trap is a superposition

$$V(\tilde{\rho}, \tilde{z}) = \sum_{i=1}^{N} V_i \phi_i(\tilde{\rho}, \tilde{z}), \qquad (8)$$

that is linear in the relative voltages applied to trap electrodes. The functions ϕ_i are solutions to Laplace's equation with boundary conditions such that $\phi_i = 1$ on the electrode that extends to ρ_i and is otherwise zero on the boundary. More precisely,

$$\phi_i(\tilde{\rho}, 0) = \begin{cases} 0, & \tilde{\rho} < \tilde{\rho}_{i-1} \\ 1, & \tilde{\rho}_{i-1} < \tilde{\rho} < \tilde{\rho}_i \,, \\ 0, & \tilde{\rho} > \tilde{\rho}_i \end{cases} \qquad (9a)$$

$$\phi_i(\tilde{\rho}, \tilde{z} \to \infty) = 0, \qquad (9b)$$

$$\phi_i(\tilde{\rho} \to \infty, \tilde{z}) = 0. \qquad (9c)$$

These potentials are independent of the voltages applied to the trap and depend only upon the relative geometry of the trap electrodes.

Standard electrostatics methods [25,26] give the ϕ_i that satisfy Laplace's equation for $\tilde{z} \geqslant 0$ and the cylindrically symmetric boundary conditions given previously,

$$\phi_i(\tilde{\rho}, \tilde{z}) = \tilde{\rho}_i \int_0^\infty dk e^{-k\tilde{z}} J_1(k\tilde{\rho}_i) J_0(k\tilde{\rho})$$

$$- \tilde{\rho}_{i-1} \int_0^\infty dk e^{-k\tilde{z}} J_1(k\tilde{\rho}_{i-1}) J_0(k\tilde{\rho}), \quad (10)$$

with the convention that $\tilde{\rho}_0 = 0$. The integrals are over products of Bessel functions. On axis,

$$\phi_i(0, \tilde{z}) = \frac{\tilde{z}}{\sqrt{(\tilde{\rho}_{i-1})^2 + \tilde{z}^2}} - \frac{\tilde{z}}{\sqrt{(\tilde{\rho}_i)^2 + \tilde{z}^2}}. \quad (11)$$

Most of the properties of a planar Penning trap can be deduced from just the potential on axis. Expressions equivalent to Eqs. (10) and (11) are in Ref. [10].

To emphasize the role of the N gaps of a planar trap we define the gap potential across gap i as the difference, $\Delta V_i \equiv V_{i+1} - V_i$. The axial potential is then given by

$$V(0, \tilde{z}) = \sum_{i=1}^N \Delta V_i \Phi_i(\tilde{z}), \quad (12)$$

$$\Phi_i(\tilde{z}) = \frac{\tilde{z}}{\sqrt{(\tilde{\rho}_i)^2 + \tilde{z}^2}} - 1, \quad (13)$$

a sum of contributions from the N gap potentials.

The axial potential can be computed exactly using Eqs. (8) and (11), or alternately from Eq. (12). Figure 4 compares an ideal harmonic axial potential to examples of axial potentials for optimized planar Penning trap configurations to be discussed. Figure 2(b) shows equipotentials spaced by V_0 for a planar Penning trap (configuration I in Table I). The equipotentials are calculated for infinitesimal gaps, but the electrodes are represented with finite gaps to make them visible. The equipotentials terminate in the gaps between electrodes. The dashed equipotentials of an ideal quadrupole are superimposed near the trap center.

E. Expansion of the trap potential

To characterize the trap potential $V(\tilde{\rho}, \tilde{z})$ for $\tilde{z} \geqslant 0$ it suffices to focus upon expansions of the potential on the $\tilde{\rho} = 0$ axis. The potential near any expansion point $\tilde{z}_0$ on this axis can be obtained using the substitution of Eq. (4). The axial potential due to one electrode [Eq. (11)] can be expanded in a Taylor series,

$$\phi_i(0, \tilde{z}) = \frac{1}{2} \sum_{k=0}^\infty C_{ki} (\tilde{z} - \tilde{z}_0)^k. \quad (14)$$

The expansion coefficients,

$$C_{ki} = \frac{2}{k!} \left[\frac{\partial^k \phi_i(0, \tilde{z})}{\partial \tilde{z}^k} \right]_{\tilde{z} = \tilde{z}_0}, \quad (15)$$

are analytic functions of the relative trap geometry, $\{\tilde{\rho}_i\}$, and the relative location of the expansion point, $\tilde{z}_0$.

The full trap potential can be similarly expanded as

$$V(0, \tilde{z}) = \frac{1}{2} V_0 \sum_{k=0}^\infty C_k (\tilde{z} - \tilde{z}_0)^k. \quad (16)$$

The one expansion coefficient needed for $k = 2$ is so far written as $V_0 C_2$. With no loss of generality we are thus free to choose
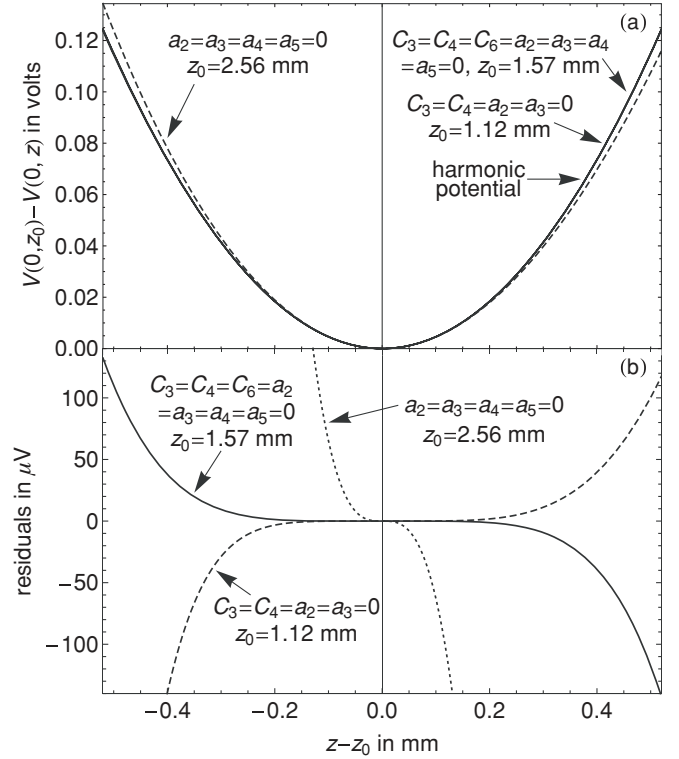

FIG. 4. (a) Trap potential on axis. (b) Difference between the trap potential and a perfect harmonic potential on axis. The labels identify optimized configurations of the sample trap (Tables I and II), using C_k from Eq. (16) and a_k from Eq. (24).

$C_2 = 1$. This determines V_0 and the C_k,

$$V_0 = \sum_{i=1}^N C_{2i} V_i, \quad (17)$$

$$C_k = \sum_{i=1}^N C_{ki} \widetilde{V}_i. \quad (18)$$

The latter equation, and the rest of this work, make frequent use of the scaled potentials $\widetilde{V}_i = V_i / V_0$. For the scaled potentials, Eq. (17) can be regarded as a constraint,

$$\sum_{i=1}^N C_{2i} \widetilde{V}_i = 1, \quad (19)$$

that an acceptable set of relative potentials must satisfy.

A trap is formed at $\tilde{z} = \tilde{z}_0$ only if there is a minimum in the potential energy $qV(0, \tilde{z})$ for a particle with charge q and mass m. The linear gradient in the potential must thus vanish at this point, whereupon

$$C_1 = \sum_{i=1}^N C_{1i} \widetilde{V}_i = 0. \quad (20)$$

Near the minimum the potential energy will then have the form $m\omega_z^2(z - z_0)^2/2$, where ω_z is the angular oscillation frequency of the trapped particle in the limit of a vanishing oscillation amplitude. Comparing to the quadratic term in Eq. (16) gives

$$\omega_z^2 = \frac{qV_0}{m\rho_1^2}, \quad (21)$$

TABLE I. Scaled parameters for the sample planar trap geometry.

	$a_2 = a_4 = 0$		$C_3 = C_4 = 0$	
	$\{\tilde{\rho}_i\} = \{1, 5.5, 7.5426\}$			
	I	II	III	IV
	Eq. (46)	Eqs. (46), (50)	Eqs. (48), (50)	Eq. (48)
$\widetilde{V}_1$	-12.2615	-26.4192	-26.4192	-31.0353
$\widetilde{V}_2$	-16.4972	-27.0861	-27.0861	-31.6642
$\widetilde{V}_3$	-79.7942	-111.1415	-111.1415	-120.1261
$\widetilde{z}_0$	2.3469	1.4351	1.4351	1.0250
C_3	-0.1516	0.0000	0.0000	0.0000
C_4	0.0287	0.0000	0.0000	0.0000
C_5	-0.0156	-0.0112	-0.0112	0.0213
C_6	0.0064	0.0000	0.0000	-0.0366
a_2	0.0000	0.0000	0.0000	0.0000
a_3	0.0000	0.0000	0.0000	0.0000
a_4	0.0000	0.0000	0.0000	-0.0343
a_5	0.0000	0.0000	0.0000	0.0000
a_6	-0.0003	-0.0039	-0.0039	-0.0095
C_{11}	-0.1205	-0.3737	-0.3737	-0.6810
C_{12}	-0.1625	0.0443	0.0443	0.3356
C_{13}	0.0521	0.0780	0.0789	0.0875
$C_{1d}^{(\text{opt})}$	-0.3280	-0.5364	-0.5364	-0.7510
$\tilde{\rho}_d^{(\text{opt})}$	3.3191	2.0295	2.0295	1.4496
γ_1	-194.15	3.45	3.45	3.50
γ_2	8.14	2.64	2.64	4.15
γ_3	-1.56	-3.12	-3.12	1.61
	Fig. 8 points		Fig. 9 points	
	Right	Left	Right	Left

the same as for the ideal case considered earlier because of our choice of V_0. Forming a trap thus requires that q and V_0 have the same sign at $\tilde{z}_0$. The sign of V_0 can be flipped if it is wrong by simply flipping the sign of all of the applied potentials.

F. Two viewpoints

Two different viewpoints of the potential expansions and equations are useful. The first is needed to analyze the performance of an N-gap trap. The second facilitates the calculation of optimized trap configurations.

The point of view that we take to analyze an N-gap trap starts with the N radii $\{\rho_i\}$ and the N applied potentials $\{V_i\}$. These are the $2N$ parameters that fully characterize such a trap. No interrelations constrain the values of these parameters, so the difference of the number of parameters and constraints is $2N$.

The axial potential is then a superposition [from Eq. (8)] of the $\phi_i(0, \tilde{z})$ from Eq. (11) with scaled radii $\{\tilde{\rho}_i\} = \{\rho_i\}/\rho_1$. The extremum of $V(0, \tilde{z})$ is the $\tilde{z}_0$ needed to evaluate the expansion coefficients $C_{ki}(\tilde{\rho}_i, \tilde{z}_0)$ using Eq. (15). All of the properties of a trap at $\tilde{z} = \tilde{z}_0$ can then be determined. The potential scale $V_0(\rho_i, \tilde{z}_0, V_i)$ is determined using Eq. (17), the axial frequency from Eq. (3), and the expansion coefficients C_k from Eq. (18). An example analysis for two existing planar Penning traps is provided in the Appendices.

The point of view we take to identify optimized planar trap configurations instead uses $2N + 2$ parameters to characterize

a planar trap. The effect of the two additional parameters is compensated by the addition of the two constraints $C_1 = 0$ and $C_2 = 1$ [from Eqs. (19) and (20)]. The difference of the number of the parameters and constraints is thus $2N$, just as for our previous analysis.

We will first seek solutions for scaled trap configurations, for which there are $2N$ parameters and two constraints. The parameters are the N scaled potentials $\{\widetilde{V}_i\}$, the $N - 1$ scaled radii $\{\tilde{\rho}_i\}$, and the scaled distance $\tilde{z}_0 > 0$. The two constraints, $C_1 = 0$ and $C_2 = 1$, are from Eqs. (19) and (20). The difference of the number of parameters and constraints for any scaled trap configuration is thus $2N - 2$. We are thus free to specify up to $2N - 2$ additional constraints on the scaled radii and scaled potentials, though not all constraints will have a set of parameters that satisfies them.

Once the $2N - 2$ scaled potentials and radii are chosen, we are then free to choose two additional parameters to bring the difference of the parameters and constraints back up to $2N$. A convenient distance scale ρ_1 and a convenient potential scale V_0 can be chosen to get a desired axial frequency [using Eq. (21)]. The radii are then $\{\rho_i\} = \rho_1\{\tilde{\rho}_i\}$, and the applied potentials are $\{V_i\} = V_0\{\widetilde{V}_i\}$.

Before applying these general considerations to two- and three-gap traps, we discuss amplitude-dependent frequency shifts since these will determine the additional constraint equations that we need to design optimized planar traps.

IV. AXIAL OSCILLATIONS

In this section we investigate the axial oscillation of a trapped particle near the potential energy minimum of a planar Penning trap. In the following sections, Secs. V and VI, we investigate optimized planar Penning traps, realized by imposing additional requirements on the design of planar traps (in addition to the two above) to make the axial oscillation of a trapped particle more harmonic.

The crucial observable for realizing a one-electron qubit is the frequency of the axial oscillation of a trapped electron. One trapped particle will be observed in the planar Penning trap only if the oscillation frequency is well enough defined to allow narrow-band radiofrequency detection methods to be used. Small changes in the particle's oscillation frequency will signal one-quantum transitions of the qubit, as has been mentioned.

For a perfect quadrupole potential, the motion of a trapped particle on the symmetry axis of the trap is perfect harmonic motion at a single oscillation frequency, ω_z, independent of the amplitude of the oscillation. For a charged particle trapped near a minimum of the nonharmonic potential expanded in Eq. (16), near $\tilde{z} = \tilde{z}_0$, the oscillation frequency depends upon the oscillation amplitude.

A. Amplitude-dependent frequency

The oscillation frequency for a particle trapped near a potential minimum within a planar Penning trap depends upon the oscillation amplitude. A derivation of this amplitude dependence starts with applying Newton's second law to get the equation of motion. For a particle of charge q and mass m

on the symmetry axis $\hat{\mathbf{z}}$ of the trap,

$$\frac{d^2}{dt^2}u + (\omega_z)^2 u + \lambda(\omega_z)^2 \sum_{k=3}^{\infty} \frac{kC_k}{2}u^{k-1} = 0, \qquad (22)$$

where $u = \tilde{z} - \tilde{z}_0$. The harmonic restoring force is presumed to be larger than the additional (unwanted) terms. The latter are labeled with a dimensionless smallness parameter λ that is taken to be unity at the end of the calculation.

Solutions are sought in the form of series expansions of the amplitude and the oscillation frequency in powers of the smallness parameter,

$$u = u_0 + \lambda u_1 + \lambda^2 u_2 + \ldots, \qquad (23a)$$
$$\omega = \omega_z + \lambda\omega_1 + \lambda^2\omega_2 + \ldots. \qquad (23b)$$

The lowest-order solution is a harmonic oscillation, with oscillation amplitude $\tilde{A}\rho_1$, for which we chose the phase $u_0 = \tilde{A}\cos(\omega t)$ with $\tilde{A} > 0$.

By assumption, the lowest-frequency Fourier component of the particle's axial motion is predominant. Fourier components at harmonics of $\omega_z(\tilde{A})$, not shown explicitly in the formula, have smaller amplitudes. The frequency contributions are determined by the requirement that no artificial driving terms resonant at angular frequency ω are introduced. This well-known method [27,28] is sometimes called the Linstedt-Poincaré method. The result is that the oscillation frequency $\omega = \omega_z(\tilde{A})$ is a function of oscillation amplitude $\tilde{A}$ for the harmonic Fourier component, given by

$$\omega_z(\tilde{A}) = \omega_z\left[1 + \sum_{k=2}^{\infty} a_k \tilde{A}^k\right]. \qquad (24)$$

At zero amplitude the oscillation frequency $\omega_z(\tilde{A}) \to \omega_z$, of course. There is no term linear in the oscillation amplitude (contrary to Ref. [10], see Appendix A).

The amplitude coefficients a_k are functions of the potential expansion coefficients C_k, each of which in turn is a function of the trap dimensions ρ_i and the potentials V_i applied to the trap electrodes.

$$a_2 = -\frac{15(C_3)^2}{16} + \frac{3C_4}{4}, \qquad (25a)$$

$$a_3 = -\frac{15(C_3)^3}{16} + \frac{3C_3C_4}{4} \qquad (25b)$$

$$= C_3 a_2, \qquad (25c)$$

$$a_4 = -\frac{2565(C_3)^4}{1024} + \frac{645(C_3)^2C_4}{128} - \frac{21(C_4)^2}{64}$$
$$- \frac{105C_3C_5}{32} + \frac{15C_6}{16}, \qquad (25d)$$

$$a_5 = -\frac{2565(C_3)^5}{512} + \frac{765(C_3)^3C_4}{64} - \frac{69C_3(C_4)^2}{32}$$
$$- \frac{15(C_3)^2C_5}{2} + \frac{3C_4C_5}{4} + \frac{15C_3C_6}{8} \qquad (25e)$$

$$= (C_5 - 2C_3C_4)a_2 + 2C_3a_4, \qquad (25f)$$

$$a_6 = -\frac{205845(C_3)^6}{16384} + \frac{159795(C_3)^4C_4}{4096}$$
$$- \frac{21039(C_3)^2(C_4)^2}{1024} + \frac{81(C_4)^3}{256} - \frac{13545(C_3)^3C_5}{512}$$

$$+ \frac{1995C_3C_4C_5}{128} - \frac{315(C_5)^2}{128} + \frac{3015(C_3)^2C_6}{256}$$
$$- \frac{57C_4C_6}{64} - \frac{315C_3C_7}{64} + \frac{35C_8}{32}, \qquad (25g)$$

$$a_7 = 3C_3a_6 + [-3(C_3)^3 - 4C_3C_4 + 2C_5]a_4 + [3(C_3)^3C_4$$
$$+ 4C_3(C_4)^2 - 2C_4C_5 - 3C_3C_6 + C_7]a_2. \qquad (25h)$$

The exact expressions derived for a_8 and a_9 take too much space to display, and are not normally needed. A convention other than $C_2 = 1$ would require that each C_k in the previous equations be replaced by C_k/C_2.

Several properties of the relationships between the C_k and a_k will be exploited for designing planar traps. Two combinations of potential expansion coefficients make $a_2 = 0$:

$$C_3 = C_4 = 0 \quad \Rightarrow \quad a_2 = 0, \qquad (26)$$
$$C_4 = \tfrac{5}{4}(C_3)^2 \quad \Rightarrow \quad a_2 = 0. \qquad (27)$$

Relationships between the a_k in Eqs. (25a)–(25f) imply

$$a_2 = 0 \Rightarrow a_3 = 0, \qquad (28)$$
$$a_2 = a_4 = 0 \Rightarrow a_2 = a_3 = a_4 = a_5 = 0. \qquad (29)$$

One set of potential coefficients that produce this remarkable suppression of the low-order a_k is

$$C_3 = C_4 = C_6 = 0 \quad \Rightarrow \quad a_2 = a_3 = a_4 = a_5 = 0. \quad (30)$$

Another is

$$C_4 = \tfrac{5}{4}(C_3)^2 \quad \text{and} \quad C_6 = -\tfrac{7}{2}C_3[(C_3)^3 - C_5]$$
$$\Rightarrow \quad a_2 = a_3 = a_4 = a_5 = 0. \qquad (31)$$

It remains to investigate whether and how any or all of these attractive combinations of C_k values can be produced by biasing a planar Penning trap.

B. Tunabilities

A change in the potential V_i applied to each electrode will change the axial frequency ω_z and will also change the amplitude dependence of the axial frequency by changing a_2. The orthogonalized hyperbolic, cylindrical, and open-access traps were designed so that the potential applied to one pair of electrodes changed the axial frequency very little while changing a_2. The potential on such compensation electrodes could then be changed to tune a_2 to zero without shifting the axial frequency out of resonance with the detectors that were needed to monitor the improvement.

We define a tunability for each electrode,

$$\gamma_i = \frac{1}{\omega_z}\frac{\partial\omega_z}{\partial V_i}\bigg/\frac{\partial a_2}{\partial V_i}. \qquad (32)$$

to quantify how useful the electrodes will be for tuning a_2. The tunabilities are defined as generalizations of the single tunability γ used to optimize the design of the orthogonalized traps.

Ideally, and this ideal was closely approximated in the orthogonalized traps, there are compensation electrodes for which $\gamma_i \approx 0$, and other electrodes for which γ_i is very large in magnitude. In Sec. VI B we will review the tunabilities that were calculated and realized for the cylindrical trap. In the

sections that follow we will compare these to what can be realized with a planar Penning trap.

C. Harmonics of the axial oscillation

The largest Fourier components for the small-amplitude motion of the trapped particle are given by

$$\tilde{z} = \tilde{z}_0 + \widetilde{A}_0 + \widetilde{A}_1 \cos(\omega t) + \widetilde{A}_2 \cos(2\omega t) + \widetilde{A}_3 \cos(3\omega t) + \dots. \tag{33}$$

By assumption, the harmonic Fourier component at frequency ω has the larger amplitude $\widetilde{A}_1 \approx \widetilde{A}$, with the harmonics then given by

$$\widetilde{A}_1 = \widetilde{A} + \frac{C_3}{2}\widetilde{A}^2 + \left[\frac{29(C_3)^2}{64} - \frac{C_4}{16}\right]\widetilde{A}^3 + \dots, \tag{34}$$

$$\widetilde{A}_2 = \frac{C_3}{4}\widetilde{A}^2 + \frac{(C_3)^2}{4}\widetilde{A}^3 + \dots, \tag{35}$$

$$\widetilde{A}_3 = \left[\frac{3(C_3)^2}{64} + \frac{C_4}{16}\right]\widetilde{A}^3 + \dots. \tag{36}$$

Insofar as $\widetilde{A} \ll 1$, these higher-order oscillation amplitudes are smaller, but they depend critically upon the low-order potential expansion coefficients as well.

D. Thermal spread in axial frequencies

The image current induced in nearby trap electrodes by a particle's axial motion is sent through the input resistance of a detection amplifier circuit. The oscillating voltage across the resistor is detected with a very sensitive cryogenic amplifier. Energy dissipated in the resistor damps the axial motion, with some damping time $(\gamma_z)^{-1}$. Section IX shows how the damping rate γ_z is related to the resistance for a three-gap trap.

The damping brings the axial motion of a trapped particle into thermal equilibrium at the effective temperature of the amplifier. It is quite challenging to achieve a low axial temperature with an amplifier turned on. For example, the electrodes of the cylindrical Penning trap were cooled to 0.1 K with a dilution refrigerator. Even with very careful heat sinking of a Metal Semiconductor Field Effect Transistor (MESFET) amplifier that was run at an extremely low bias current, however, the axial temperature with the amplifier operating was still $T_z = 5.2$ K [29]. We then used feedback cooling to bring the axial temperature as low as 0.85 K [29]. A lower axial temperature was obtained, but only by switching the

amplifier off during critical stages of the measurement of the electron magnetic moment. For the estimates that follow we will assume an axial temperature of 5 K, but stress that much higher axial temperatures are very hard to avoid.

What has prevented the observation of one electron in a planar trap so far is the large amplitude dependence of the axial frequency in such traps. Thermal fluctuations of the particle's axial energy make the particle oscillate at a range of Fourier components, $\Delta\omega_z$. In the cylindrical trap of Fig. 1(c) this spread in frequencies is less than the damping width, $\Delta\omega_z < \gamma_z$. For planar traps so far the thermal spread of axial oscillation frequencies is much broader than the damping width, $\Delta\omega_z \gg \gamma_z$.

As a measure of the thermal width we will consider only the lowest-order contribution

$$\frac{\Delta\omega_z}{\omega_z} \approx |a_2| \frac{k_B T_z}{\frac{1}{2}m\omega_z^2 \rho_1^2}. \tag{37}$$

It should be possible to calculate neglected higher-order contributions if correlations are considered carefully, but this lowest-order expression suffices for our purposes.

The tables that follow report the lowest-order thermal widths $\Delta f_z = \Delta\omega_z/(2\pi)$ and the damping widths $\gamma_z/(2\pi)$ in Hz. Vanishing values of Δf_z thus mean that $a_2 = 0$, whereupon there is typically not much thermal broadening of the damping width. However, higher-order contributions ensure that there is always a nonvanishing thermal width.

V. TWO-GAP TRAPS

A minimal requirement for a useful trap is that it be possible to bias its electrodes to make the leading contribution to the amplitude dependence of the axial frequency vanish, $a_2 = 0$. We show here that this is not possible with a two-gap ($N = 2$) planar trap.

A scaled two-gap planar trap is characterized by $2N = 4$ parameters: $\tilde{\rho}_2$, $\widetilde{V}_1$, $\widetilde{V}_2$, and $\tilde{z}_0$. These parameters must satisfy the two constraints $C_1 = 0$ and $C_2 = 1$ [of Eqs. (19) and (20)]. The difference of the number of parameters and constraints is thus $2N - 2 = 2$. Consistent with this, we can solve for any two of the parameters in terms of the other two.

Unfortunately, if the additional constraint $a_2 = 0$ is added then there are no sets of parameters that are solutions. An explicit demonstration that a_2 cannot be made to vanish comes from solving for $\widetilde{V}_1$ and $\widetilde{V}_2$ in terms of $\tilde{z}_0$ and $\tilde{\rho}_2$ using the two constraint equations. These solutions determine

$$C_3 = \frac{-9(\tilde{z}_0)^4 + (\tilde{\rho}_2)^2 - 4(\tilde{z}_0)^2[1 + (\tilde{\rho}_2)^2]}{3[\tilde{z}_0 + (\tilde{z}_0)^3][(\tilde{z}_0)^2 + (\tilde{\rho}_2)^2]}, \tag{38}$$

$$C_4 = \frac{5[15(\tilde{z}_0)^6 + 12(\tilde{z}_0)^4[1 + (\tilde{\rho}_2)^2] - 3[(\tilde{\rho}_2)^2 + (\tilde{\rho}_2)^4] + (\tilde{z}_0)^2[4 - 5(\tilde{\rho}_2)^2 + 4(\tilde{\rho}_2)^4]]}{12[1 + (\tilde{z}_0)^2]^2[(\tilde{z}_0)^2 + (\tilde{\rho}_2)^2]^2}, \tag{39}$$

$$a_2 = -\frac{5[36(\tilde{z}_0)^8 + (\tilde{\rho}_2)^4 + 36(\tilde{z}_0)^6[1 + (\tilde{\rho}_2)^2] + (\tilde{z}_0)^2[(\tilde{\rho}_2)^2 + (\tilde{\rho}_2)^4] + (\tilde{z}_0)^4[4 + 29(\tilde{\rho}_2)^2 + 4(\tilde{\rho}_2)^4]]}{48(\tilde{z}_0)^2[1 + (\tilde{z}_0)^2]^2[(\tilde{z}_0)^2 + (\tilde{\rho}_2)^2]^2}. \tag{40}$$
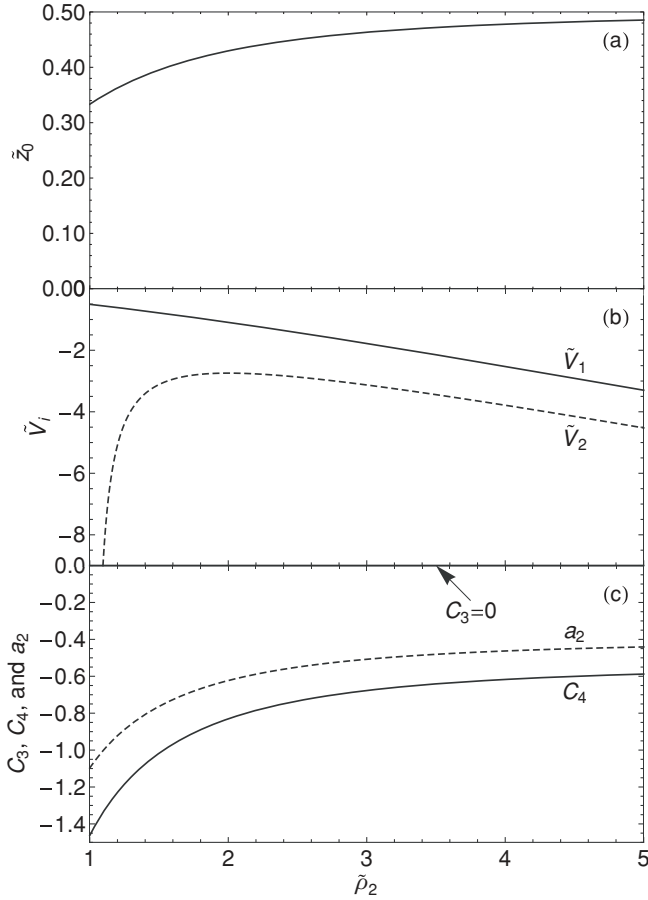
FIG. 5. Parameters of two-gap traps that make $C_3 = 0$ as a function of $\tilde{\rho}_2$.

The amplitude coefficient a_2 is explicitly negative for all values of $\tilde{z}_0$ and $\tilde{\rho}_2$, and it only approaches zero in the not-so-useful limit that $\tilde{z}_0 \to 0$.

The best that can be done with a two-gap trap is to use $C_3 = 0$ as a third constraint on the four parameters, $\tilde{V}_1$, $\tilde{V}_2$, $\tilde{z}_0$, and $\tilde{\rho}_2$. Only the analytic solution for $\tilde{z}_0$ is simple enough to display here,

$$\tilde{z}_0 = \frac{1}{3}\sqrt{\sqrt{4(\tilde{\rho}_2)^4 + 17(\tilde{\rho}_2)^2 + 4} - 2(\tilde{\rho}_2)^2 - 2}. \quad (41)$$

Figure 5 shows how the parameters of two-gap traps depend upon $\tilde{\rho}_2$.

Two-gap traps are not so useful given that it is not possible to do better than make $C_3 = 0$. It is not possible to make $a_2 = 0$. For the remainder of our discussion of planar traps we concentrate on three-gap traps since these have much better properties.

VI. OPTIMIZED THREE-GAP TRAPS

A. Overview

The goal of our optimization of a planar trap is to reduce the amplitude dependence of the axial oscillation frequency of a trapped particle to a manageable level so that the trapped particle's oscillation energy is in a narrow range of Fourier components. Otherwise, the oscillation energy will be broadened by noise-driven amplitude fluctuations to a broader range of Fourier components. The signal induced by the more harmonic axial oscillation can then be filtered with a narrow-band detector that rejects nearby noise components, making possible the good signal-to-noise ratio needed to detect the small frequency shifts that signal one-quantum transitions.

The dependence of the axial frequency $\omega_z(\widetilde{A})$ on the oscillation amplitude $\widetilde{A} = A/\rho_1$ is given by

$$\frac{\omega_z(\widetilde{A}) - \omega_z}{\omega_z} = 1 + a_2\widetilde{A}^2 + a_3\widetilde{A}^3 + a_4\widetilde{A}^4$$
$$+ a_5\widetilde{A}^5 + a_6\widetilde{A}^6 + \dots, \quad (42)$$

the low-order terms from Eq. (24). Since $\widetilde{A} \ll 1$, the lowest-order amplitude coefficient a_2 is the most important, followed by a_3, and so on. Each of the coefficients a_k is a function [given in Eq. (25)] of the potential expansion coefficients. Each of these is determined by the geometry and the applied trapping potentials, which must then be determined.

As discussed more generally in Sec. III F, a scaled three-gap planar Penning trap configuration is specified by $2N = 6$ parameters: $\tilde{\rho}_2$, $\tilde{\rho}_3$, $\widetilde{V}_1$, $\widetilde{V}_2$, $\widetilde{V}_3$, and $\tilde{z}_0$. These can be chosen to realize desired properties of a trap. These parameters must satisfy the two constraint equations $C_1 = 0$ and $C_2 = 1$ [Eqs. (19) and (20)]. The difference of the number of parameters and the number of constraints is thus $2N - 2 = 4$. The challenge is to identify up to four useful sets of constraint equations for which solutions exist.

B. What is needed?

To estimate what is needed to observe a single trapped electron it is natural to look to the demonstrated properties of the cylindrical trap used to observe the one-quantum transitions we seek to emulate. The electrodes of a cylindrical trap are invariant under reflections $z \to -z$ about the position of the trapped particle. This symmetry is never true for a planar Penning trap.

The first consequence of the reflection symmetry is that the odd-k expansion coefficients C_k vanish. The second is that the low-order, odd-k a_k vanish as well, since these are proportional to the C_k with odd k. For a cylindrical trap the frequency expansion coefficients a_k of Eq. (25) thus simplify to

$$a_2 = \tfrac{3}{4}C_4, \quad (43a)$$
$$a_3 = 0, \quad (43b)$$
$$a_4 = \tfrac{15}{16}C_6 - \tfrac{21}{64}(C_4)^2, \quad (43c)$$
$$a_5 = 0. \quad (43d)$$

The odd-order a_k thus vanish naturally for an ideal cylindrical Penning trap.

Care must be taken in making quantitative comparisons between the planar traps and the cylindrical trap. Amplitudes and distances in the cylindrical trap were naturally scaled by the larger value of $d = 3.54$ mm [16,30] rather than by $\rho_1 = 1.09$ mm as in the sample trap considered here, for trap configurations that produce the same axial frequency. The conversion between the $C_k^{(\text{cyl})}$ for the cylindrical trap [30,31]

and the C_k for the planar trap is given by

$$C_k = \left(\frac{\rho_1}{d}\right)^{k-2} \frac{C_k^{(cyl)}}{C_2^{(cyl)}}. \tag{44}$$

We apply this conversion to reported values for the cylindrical trap for the rest of this section.

The amplitude dependence of the axial frequency is reduced for the cylindrical Penning trap by adjusting a single compensation potential applied to a pair of compensation electrodes. The adjustment changes primarily C_4, but also C_6 to a lesser amount. The adjustment continues until $C_4 \approx 0$, whereupon $C_6 \approx -0.0008$. The frequency coefficients are then found using the appropriately converted C_k in Eq. (25). This gives $a_2 = a_3 = a_5 = 0$ and $a_4 = -0.0007$.

The resulting frequency-versus-amplitude curve is shown in Fig. 6 for $\omega_z/(2\pi) = 64$ MHz, and the corresponding thermal spread of axial frequencies is $\Delta f_z = 0$ Hz since $a_2 = 0$. The compensation potential is typically then adjusted slightly away from $C_4 = 0$ to make the axial frequency insensitive to small fluctuations about a particular oscillation amplitude [32].

In practice, $C_4 = 0$ is not realized exactly, but $|C_4| < 10^{-5}$ is typically achieved. If $C_4 = -10^{-5}$, and $C_6 = -0.0008$ as before, then the amplitude coefficients are $a_2 = -8 \times 10^{-6}$, $a_4 = -0.0007$, and $a_3 = a_5 = 0$, the thermal spread of axial frequencies is 0.5 Hz, and the frequency-versus-amplitude curve is as shown in Fig. 6.

The cylindrical trap is designed so that the axial frequency is much more insensitive to the tuning compensation potential than to the potential applied to make the main trapping potential. If we define the endcap electrode potential to be

our zero of potential, the γ_i factors are $\gamma_{ring} = -141$ and $\gamma_{comps} = 0.032$. The latter would have the value $\gamma_{comps} = 0$ for the "orthogonalized" design for the cylindrical trap except for the unavoidable imperfections of a real laboratory trap.

C. Previous three-gap traps

In marked contrast to the cylindrical trap within which the one-quantum transitions of a single electron were observed, the planar traps attempted so far were not designed to make $a_2 = 0$ and were not biased to make even $C_3 = 0$. It is thus not so surprising that attempts to observe one electron in a planar Penning trap have not succeeded.

In fact, Fig. 7 shows that the three-gap trap geometries tried so far (crosses) are outside of all of the shaded regions that we use to identify optimized trap geometries. The best that could have been done for the earlier planar traps would have been to make $C_3 = 0$. In fact, any trap geometry represented in the upper triangular region of Fig. 7 can be tuned to make C_3 vanish. Appendices B and C look more closely at the design of earlier planar Penning traps and suggest that these were not biased to make $C_3 = 0$.

D. Optimize to $a_2 = a_3 = a_4 = a_5 = 0$

For a scaled three-gap trap we must choose six parameters ($\tilde{\rho}_2$, $\tilde{\rho}_3$, $\tilde{V}_1$, $\tilde{V}_2$, $\tilde{V}_3$, and $\tilde{z}_0$) that solve the constraints of Eqs. (19) and (20). Our preferred path to optimization starts from adding
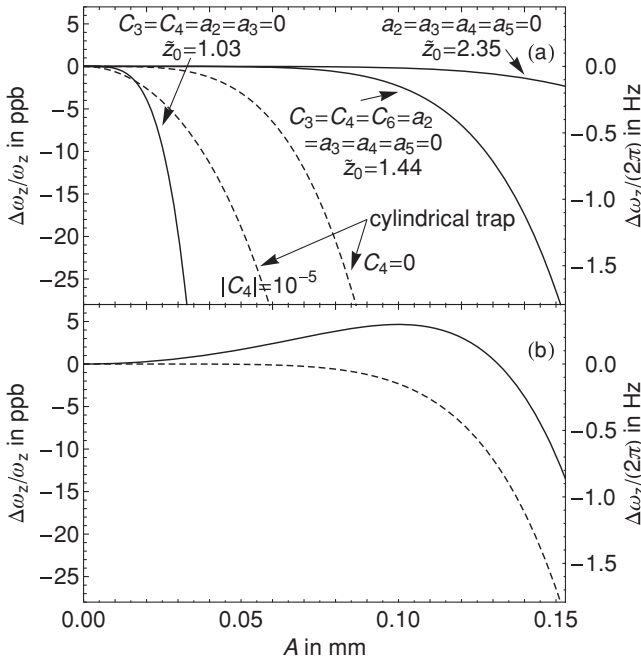

FIG. 6. (a) Amplitude dependence of $\omega_z(A) \approx 2\pi 64$ MHz for optimized configurations of the sample trap (Table I) is comparable or smaller than for the cylindrical trap. (b) Slight adjustments in the applied potentials minimize the dependence of ω_z upon fluctuations about a large oscillation amplitude (solid) rather than for small oscillation amplitudes (dashed).
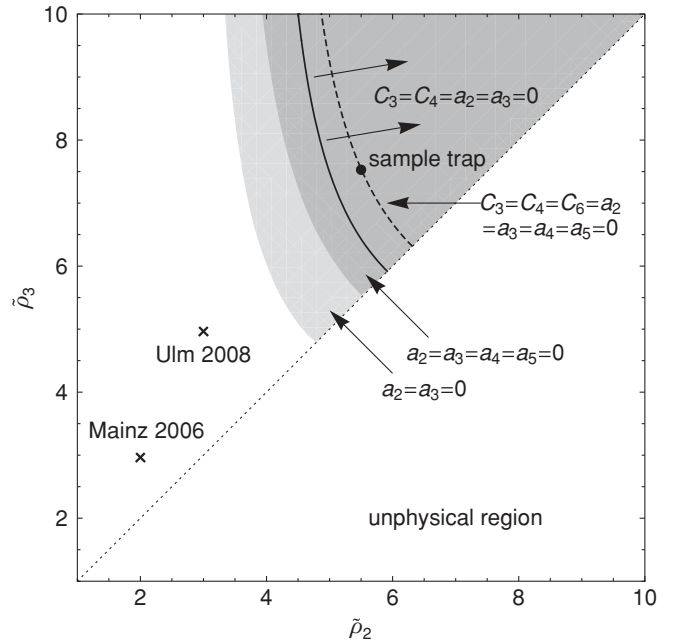

FIG. 7. The shaded regions for which the indicated a_k can be made to vanish for a three-gap planar Penning trap, along with the region and the curve for which the indicated C_k can alternatively be made to vanish. To be avoided is the shaded area near the diagonal boundary $\tilde{\rho}_2 = \tilde{\rho}_3$ where there is a rather strong and sensitive cancellation between the effect of the potentials V_2 and V_3. No optimized traps are possible in the unshaded region, with the the earlier traps (crosses) at Mainz [11] and Ulm [13] as examples.
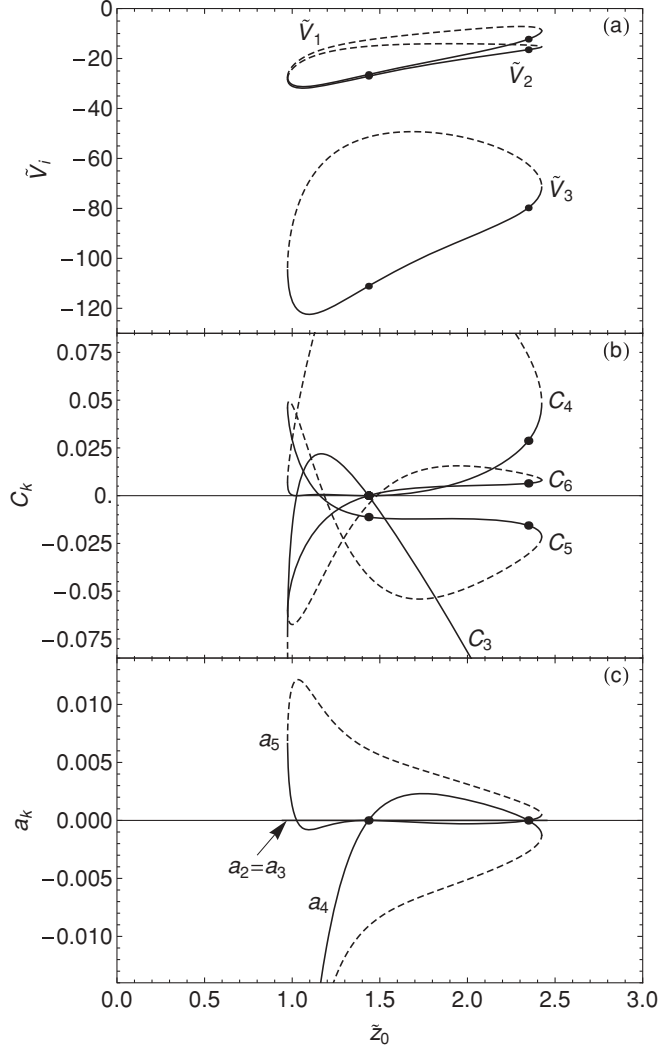
FIG. 8. (a) Scaled potentials applied to the sample trap electrodes to make a trap with $a_2 = 0$ as a function of the position $\tilde{z}_0$ of the axial potential minimum. (b) The corresponding C_k. (c) The corresponding a_k.

the constraints

$$C_1 = 0, \tag{45a}$$

$$C_2 = 1, \tag{45b}$$

$$a_2 = a_3 = 0. \tag{45c}$$

What appear here to be four constraints are actually three constraints because $a_3 = 0$ follows from $a_2 = 0$ via Eq. (25c).

The difference of the number of parameters and constraints is three. Where solutions exist, we might thus expect them to be functions of the two parameters that specify the relative geometry, and that a range of $\tilde{z}_0$ might be possible. The shaded area in Fig. 7 represents the relative geometries for which there are solutions. Solutions also do exist for a range of $\tilde{z}_0$ values, as illustrated in Fig. 8 for our sample trap geometry. The solutions are double-valued because the third constraint equation is quadratic in the scaled potentials $\tilde{V}_1$, $\tilde{V}_2$, and $\tilde{V}_3$. The solid and dashed curves distinguish the two branches.

The left and right points in Fig. 8, with detailed properties in columns I and II of Tables I and II, are trap configurations

TABLE II. One set of absolute values for the sample planar trap geometry. The broadening Δf_z is for a 5 K thermal distribution of axial energies. The damping widths $\gamma_z/(2\pi)$ are for the numbered electrode connected to $R = 100\,\text{k}\Omega$. Thermal frequency spreads Δf_z below 1 Hz will be very difficult to realize in practice owing to imperfections in real traps.

	$\{\rho_i\} = \{1.0909, 6, 8.2283\}$ mm				
	$a_2 = a_4 = 0$		$C_3 = C_4 = 0$		
	I	II	III	IV	
	Eq. (46)	Eqs. (46), (50)	Eqs. (48), (50)	Eq. (48)	
ρ_1	1.0909	1.0909	1.0909	1.0909	mm
z_0	2.5603	1.5655	1.5655	1.1182	mm
$\rho_d^{(\text{opt})}$	3.6208	2.2140	2.2140	1.5814	mm
f_z	64	64	64	64	MHz
V_0	-1.0941	-1.0941	-1.0941	-1.0941	V
V_1	13.4158	28.9064	28.9064	33.9572	V
V_2	18.0504	29.6361	29.6361	34.6452	V
V_3	87.3065	121.6051	121.6051	131.4355	V
Δf_z	0.0	0.0	0.0	0.0	Hz
$1:\gamma_z$	$2\pi\,1.37$	$2\pi\,13.16$	$2\pi\,13.16$	$2\pi\,43.70$	s^{-1}
$2:\gamma_z$	$2\pi\,2.49$	$2\pi\,0.19$	$2\pi\,0.19$	$2\pi\,10.61$	s^{-1}
$3:\gamma_z$	$2\pi\,0.26$	$2\pi\,0.57$	$2\pi\,0.57$	$2\pi\,0.72$	s^{-1}
$d:\gamma_z^{(\text{opt})}$	$2\pi\,10.14$	$2\pi\,27.11$	$2\pi\,27.11$	$2\pi\,53.14$	s^{-1}
	Fig. 8 points		Fig. 9 points		
	Right	Left	Right	Left	

that satisfy the more stringent set of constraints

$$C_1 = 0, \tag{46a}$$

$$C_2 = 1, \tag{46b}$$

$$a_2 = a_3 = a_4 = a_5 = 0. \tag{46c}$$

What appear to be six constraints on the six parameters are actually four constraints in light of Eq. (29). The difference of the number of parameters and constraints is thus two. Where solutions exist we will thus regard them as functions of the relative geometry, $\tilde{\rho}_2$ and $\tilde{\rho}_3$, which will then determine a particular value of $\tilde{z}_0$. The darkly shaded region in Fig. 7 shows the relative geometries for which solutions can be found.

For the solution that is the right point in Fig. 8 none of the potential coefficients C_3, C_4, C_5, and C_6 vanish. The axial potential in Fig. 4 is thus clearly different from a harmonic oscillator potential. Since $C_3 \neq 0$ the amplitude of the second harmonic of the axial oscillation is the lowest-order term from Eq. (35),

$$\frac{\tilde{A}_2}{\tilde{A}_1} = \frac{C_3}{4}\tilde{A} + \dots. \tag{47}$$

The amplitude of this second harmonic should still be relatively small insofar as $\tilde{A} = A/\rho_1$ is small.

We discuss the solution that is the left point in Fig. 8 and column II in Tables I and II in Sec. VI F.

E. Optimize to $C_3 = C_4 = a_2 = a_3 = 0$

A second path to optimizing the six parameters for a scaled trap configuration starts with adding the constraint $C_3 = 0$ to the two requirements for a trap, $C_1 = 0$ and $C_2 = 1$ [Eqs. (19) and (20)]. All three constraint equations are then linear in the scaled potentials $\tilde{V}_1$, $\tilde{V}_2$, and $\tilde{V}_3$, yielding single-valued
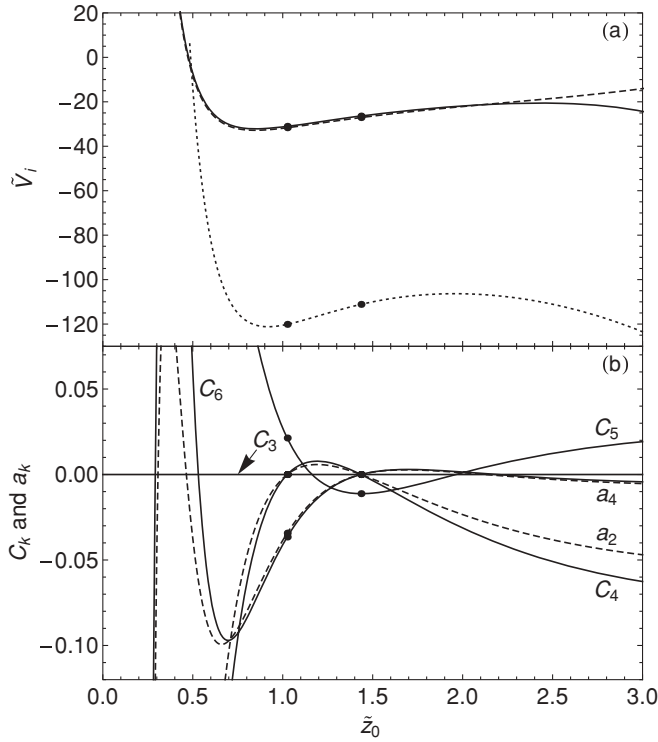
FIG. 9. (a) Scaled potentials applied to our sample trap electrodes to produce a trap with $C_3 = 0$ as a function of $\tilde{z}_0$. (b) The resulting C_k and a_k.

solutions for a given $\tilde{z}_0$, $\tilde{\rho}_2$, and $\tilde{\rho}_3$. There are three more parameters than constraints. Solutions that give $C_3 = 0$ are possible for any relative geometry. The traps can be biased to make a range of $\tilde{z}_0$ values. For our sample trap geometry, the scaled potentials are plotted as a function of $\tilde{z}_0$ in Fig. 9. The resulting C_k and a_k are shown as well.

The axial potential is more harmonic at the two points in Fig. 9, both of which satisfy the more stringent set of constraints,

$$C_1 = C_3 = C_4 = 0, \tag{48a}$$

$$C_2 = 1, \tag{48b}$$

$$a_2 = a_3 = 0. \tag{48c}$$

What appear to be six constraints on the six parameters for the scaled trap are actually four [since Eq. (48c) follows from Eqs. (48a) and (48b) via Eqs. (25a)–(25c)]. There are thus only two more parameters than constraints. Various relative trap geometries can thus be biased to satisfy this set of constraints, as represented by the solid boundary and arrows labeled $C_3 = C_4 = a_2 = a_3 = 0$ in Fig. 7, and $\tilde{z}_0$ is thus determined for each relative geometry. Note that although this region lies within the shaded area for which $a_2 = a_3 = a_4 = a_5 = 0$ can be realized, in general it is not possible to satisfy both sets of constraints simultaneously.

For the sample trap geometry, two of the applied potentials are nearly the same, making this nearly a two-gap trap, but the slight potential difference is needed. More details about these solutions are in columns III and IV of Tables I and II. Compared to the optimized configuration in Eq. (46), the optimization of Eq. (48) has a more harmonic potential (Fig. 4) but a less

good suppression of the amplitude dependence of the axial frequency as long as $a_4 \neq 0$ and $a_5 \neq 0$.

Any solution with $C_3 = C_4 = 0$ (including the two points in Fig. 9 and columns III and IV in Tables I and II, as well as the left solution point in Fig. 8 column II in Tables I and II described in the following) has a suppressed harmonic content compared to Eq. (47), with

$$\frac{\widetilde{A}_2}{\widetilde{A}_1} = \frac{5C_5}{12}\widetilde{A}^3 + \dots, \tag{49}$$

from Eqs. (34) and (35). The amplitude of higher harmonics is suppressed by additional powers of $\widetilde{A}$.

We discuss the solution that is the right point in Fig. 9 and column III in Tables I and II in the following section.

F. Harmonic optimization

The highest level of optimization is for traps that are harmonic in that $C_3 = C_4 = 0$, as well as having the remarkable suppression of the amplitude dependence of the axial frequency that comes by adding $C_6 = 0$ [Eq. (30)]. For this optimized harmonic configuration

$$C_1 = C_3 = C_4 = C_6 = 0, \tag{50a}$$

$$C_2 = 1, \tag{50b}$$

$$a_2 = a_3 = a_4 = a_5 = 0. \tag{50c}$$

What appear to be nine constraints are actually five [because Eqs. (50c) follows from Eqs. (50a) and (50b) via Eqs. (25)]. There is thus one more parameter to chose ($\tilde{\rho}_2$, $\tilde{\rho}_3$, $\widetilde{V}_1$, $\widetilde{V}_2$, $\widetilde{V}_3$, and $\tilde{z}_0$) than there are constraints. The free parameter leads to a range of possible relative geometries (the dashed line in Fig. 7). Missing from Eq. (50) is $C_5 = 0$ since there are no solutions when this constraint is added.

Our sample trap (filled circle in the dashed line in Fig. 7) is one example. For it, the left solution point in Fig. 8 and the right solution point in Fig. 9 are actually the same configuration, as is obvious from columns II and III of Tables I and II. This convergence of two solutions happens only for traps with relative geometries on the dashed line in Fig. 7. For other traps in the shaded region where $a_2 = a_4 = 0$ can be satisfied, these two solutions remain distinct, and the highly optimized constraints of Eq. (50) cannot be satisfied for any choice of the trap potentials.

The optimized harmonic trap configurations (Fig. 10) involve only a very narrow range of scaled distances $\tilde{z}_0$ from the electrode plane to the axial potential minimum. The scaled potentials needed are shown in Fig. 10(b). The leading departure from a harmonic potential is described by $C_5 = -0.011$ [Fig. 10(b)]. As mentioned, we find no solutions to the constraint equations if a vanishing C_5 is required.

The highly optimized properties of Eq. (50) are an optimized harmonic configuration in that the leading departures from a harmonic axial potential vanish because $C_3 = C_4 = 0$ at the same time that the amplitude dependence of the axial frequency is strongly suppressed. A particle's axial oscillation will thus have a very small amplitude at the overtones of the fundamental harmonic, as given by Eq. (49), with the amplitude of higher harmonics suppressed by additional powers of $\widetilde{A}$.
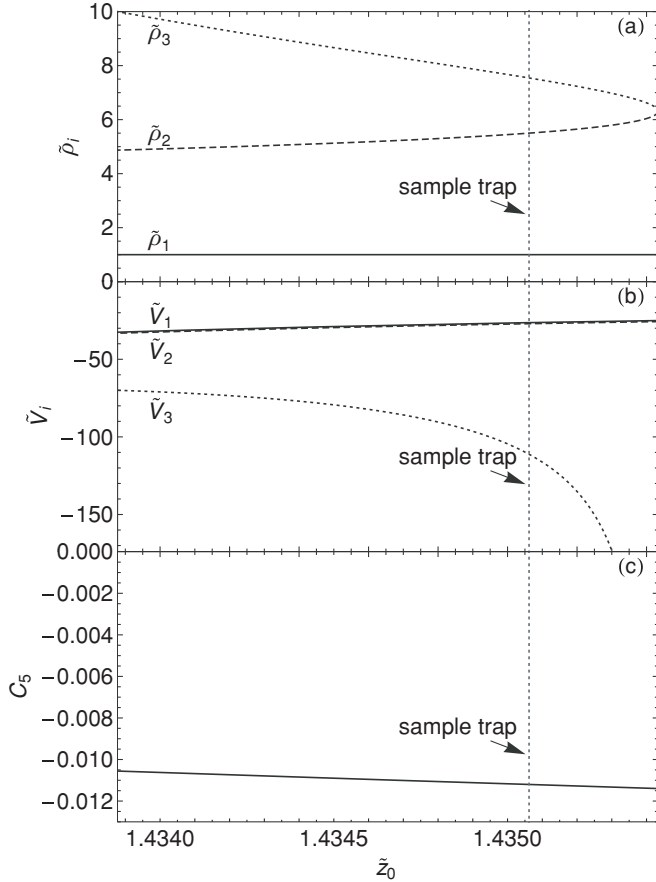
FIG. 10. (a) An optimized harmonic trap [Eq. (50)], as illustrated using our sample trap geometry, is possible with only a small range of $\tilde{z}_0$ values and relative geometries. (b) The required scaled potentials. (c) Values of the nonzero C_5.
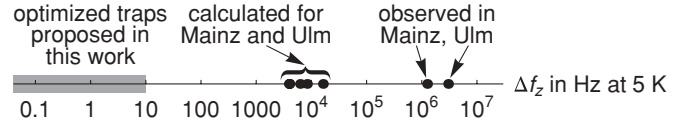

FIG. 11. Comparison of the frequency widths calculated for optimized planar traps with a 5 K axial temperature. The imperfections of a real planar trap will likely make it difficult to realize widths below 1 Hz for an axial frequency of 64 MHz.

VII. LABORATORY PLANAR TRAPS

Planar Penning traps put into service in the laboratory will not have the ideal properties described in the previous sections of this work. A real trap does not have gaps of negligible width, does not have an electrode plane that extends to infinity, does not have conducting boundaries at an infinite distance above the electrode plane and at an infinite radius, and will not have exactly the ideal dimensions and the perfect cylindrical symmetry that are being approximated. None of these have large effects. However, the result is that the potentials applied to the electrodes of a real laboratory trap will need to be adjusted a bit from the ideal planar trap values to compensate for the unavoidable deviations and imperfections.

The effect of nonnegligible gaps is calculated in Sec. VII A. The effect of a finite electrode plane and a finite conducting radial enclosure is discussed in Sec. VII C. Imperfections in the trap dimensions and symmetry are dealt with in Sec. VII D using simple estimates that proved adequate for the design of earlier traps. These estimates are used to discuss the tunning of the trap potentials required to compensate for imperfections of this order (Sec. VII E).

G. Comparing amplitude-dependent frequency shifts

The optimized trap configurations greatly reduce the amplitude dependence of the axial oscillation frequency. Avoiding frequency fluctuations caused by noise-driven amplitude fluctuations is critical to resolving the small frequency shifts that signal one-quantum cyclotron and spin transitions.

One way to compare the optimized configurations is in Fig. 6. The axial frequency shift is shown as a function of oscillation amplitude for the three optimized configurations of the sample trap. For one electron in the cylindrical trap an oscillation amplitude of 0.1 mm was large and easily detectable.

Another figure of merit is the frequency broadening for the thermally driven axial motion of a trapped particle, which was discussed in Sec. IV D. We use the 5 K axial temperature realized and measured for a cylindrical Penning trap cooled by a dilution refrigerator [29], though it should be noted that realizing such a low detector temperature is a challenging undertaking. Each trap configuration can thus be characterized by the thermal broadening of the axial resonance frequency, as indicated in Fig. 11. Imperfections in real planar traps and instabilities in applied potentials will likely make it difficult to get thermal widths much less than 1 Hz for an axial frequency of 64 MHz.

A. Gaps between electrodes

Small gaps of some width w between electrodes are unavoidable, of course. As long as $w \ll z_0$, the potential variation caused by the gaps at the position of the trapped particle should be small since it should diminish exponentially with an argument that goes as w/z_0. We assume that the gaps between electrodes are deeper than they are wide since this is needed to screen the effect of any stray charges on the insulators that keep the electrodes apart.

Solving exactly for the trapping potential using boundary conditions that include deep gaps between the electrodes is a challenging undertaking. Instead we use a simple and approximate boundary condition that was used to demonstrate the small effect of the gaps in a cylindrical trap [16]. We take the potential in the electrode plane across each gap to vary linearly between the potentials of the two electrodes. The potential is thus determined everywhere in the electrode plane by the potentials on the electrodes.

The basis of this approximation is illustrated by the equipotentials shown for a planar trap in Fig. 2(b) [and later in Figs. 12(b), 14(b), and 16(b)]. All the equipotentials from the trapping volume must connect to equipotentials within the gaps. Deep within a small but deep gap the equipotentials will locally be similar to the equipotentials between parallel plates, the plates being the vertical electrode walls within the gap. The equipotentials will remain roughly parallel until they

rise above the electrode plane, whereupon they will spread. We make the approximation that in the electrode plane the potential in the gap varies linearly with radius between the voltages applied to the two electrodes that are separated by the gap. Since the effect of the gaps is already small a better approximation should not be needed.

The completely specified electrode plane boundary is thus given by the electrode boundaries and the linear change of potential between them at the gaps of width w_i (with $\widetilde{w}_i = w_i/\rho_1$) centered at radius ρ_i. The solution to Laplace's equation on axis then becomes

$$V^{\text{gap}}(0, z) = \sum_{i=1}^{N} \Delta V_i \Phi_i(\tilde{z}), \tag{51}$$

$$\Phi_i(\tilde{z}) = \frac{\tilde{z}}{\widetilde{w}_i} \sinh^{-1}\left(\frac{\tilde{\rho}_i + \widetilde{w}_i/2}{\tilde{z}}\right)$$
$$- \frac{\tilde{z}}{\widetilde{w}_i} \sinh^{-1}\left(\frac{\tilde{\rho}_i - \widetilde{w}_i/2}{\tilde{z}}\right) - 1. \tag{52}$$

In the limit of vanishing gap widths this potential becomes the potential of an ideal planar trap in Eqs. (12) and (13).

Following the procedure outlined earlier (Sec. VI), this potential is expanded about $\tilde{z} = \tilde{z}_0$. Sets of parameters that satisfy reasonable constraint equations identify the optimized trap configurations that greatly reduce the amplitude dependence of the axial frequency and make the trap potential more harmonic. We get four optimized configurations, as before, but with applied potentials that are slightly shifted.

Biasing a trap with a finite gap width as if it was an ideal planar trap with no gap width is one approach. Table III shows the C_k and a_k when ideal trap biases (from Tables I and II) are applied to the sample trap with $w = 50\ \mu$m gap widths. The broadening of the axial frequency Δf_z for a thermal distribution of axial frequencies is still small enough that it should not prevent observing one electron in a trap with such gaps.

TABLE III. Gaps between the electrodes of the sample trap when the potentials for an ideal planar trap (from Tables I and II) are applied produce different C_k and a_k. The gap width is $w = 0.002$ in $= 50\ \mu$m.

	{$\widetilde{\rho}_i$} = {1, 5.5, 7.5426}				
	$a_2 = a_4 = 0$		$C_3 = C_4 = 0$		
	I	II	III	IV	
	Eq. (46)	Eqs. (46), (50)	Eqs. (48), (50)	Eq. (48)	
$\widetilde{z}_0$	2.3469	1.4351	1.4351	1.0250	
C_3	−0.1516	0.0000	0.0000	0.0000	
C_4	0.0287	0.0000	0.0000	0.0001	
C_5	−0.0156	−0.0112	−0.0112	0.0213	
C_6	0.0064	0.0000	0.0000	−0.0365	
a_2	0.0000	0.0000	0.0000	0.0000	
a_3	0.0000	0.0000	0.0000	0.0000	
a_4	0.0000	0.0000	0.0000	−0.0342	
a_5	0.0000	0.0000	0.0000	0.0000	
a_6	−0.0003	−0.0039	−0.0039	−0.0095	
Δf_z @ 5 K	0.3	0.3	0.3	2.7	Hz

TABLE IV. Gaps of width $w = 0.002$ in $= 50\ \mu$m between the electrodes of our sample trap shift the scaled and absolute potentials that must be applied to obtain the optimized trap configurations. The shifts are with respect to the values calculated for a vanishing gap width in Tables I and II.

	{$\widetilde{\rho}_i$} = {1, 5.5, 7.5426}				
	$a_2 = a_4 = 0$		$C_3 = C_4 = 0$		
	I	II	III	IV	
	Eq. (46)	Eqs. (46), (50)	Eqs. (48), (50)	Eq. (48)	
$\delta \widetilde{V}_1$	−0.0008	0.0015	0.0015	−0.0076	
$\delta \widetilde{V}_2$	−0.0006	0.0014	0.0014	−0.0076	
$\delta \widetilde{V}_3$	0.0034	0.0048	0.0048	−0.0157	
δV_1	0.0009	−0.0016	−0.0016	0.0083	V
δV_2	0.0006	−0.0015	−0.0015	0.0083	V
δV_3	−0.0037	−0.0053	−0.0053	0.0172	V
Δf_z @ 5 K	0.0	0.0	0.0	0.0	Hz

Shifting the potentials applied to the electrodes improves the C_k and a_k, as indicated in Table IV. However, the predicted thermal widths then become smaller than what imperfections (discussed in Sec. VII D) will likely allow us to attain, so this adjustment is not really needed.

The small size of these coefficients illustrates that realistic gaps between the electrodes of a trap as large as our sample trap pose no threat to realizing a planar Penning trap. Simply biasing the trap as if it were a trap with vanishing gap widths suffices. However, as planar traps get smaller the gaps will likely be relatively larger with respect to the trap dimensions. The use of Eqs. (51) and (52) will then be required.

B. Practical limitations on gaps

Two practical considerations are associated with gaps between electrodes. Both can make the difference between a trap that works and one that does not. Both are difficult to calculate.

The first is that charges that accumulate on the insulators in the gaps between the electrodes can substantially modify the trapping potential. When the trap is cooled to 4 K or below, these charges can remain for days. Such charges have made some traps in our laboratory completely unusable, but no systematic study has been undertaken.

There are only two solutions that we know of. Careful loading and operation procedures can minimize the number of charges that build up on the insulators. Also, thick metal electrodes with narrow gaps make it more difficult for charges to reach the insulating substrate at the bottom of the slits between electrodes. Any charges that do collect on the insulator will be screened by metal surfaces to either side of the gaps.

As mentioned in the Appendices, both the Mainz and Ulm traps had exposed insulators in gaps that were not screened because the gaps were wider than they were deep. Charges on the insulating substrates that are exposed in the gaps of these traps may well have contributed to the broad frequency spreads that were observed. Improved traps with much better screening

of the insulator at the bottom of the gaps seem possible but have yet to be used with trapped particles.

The second practical consideration involving gaps between electrodes becomes more serious with decreasing gap width. We have observed currents between polished gold-plated trap electrodes separated by small gaps. These field emission currents [33–36] grow exponentially with the difference in potential across the gap.

Trap designs that limit the size of the gap potentials are one solution. For three-gap traps, $\Delta V_3 = 0 - V_3$ is generally the largest of the gap potentials. It can generally be reduced by decreasing the radial width of the second electrode, $\rho_2 - \rho_1$, and increasing the radial width of the third electrode, $\rho_3 - \rho_2$. We will see in Sec. VIII A that a planar trap with a conducting plane above it will permit an optimized trap with lower gap potentials. Other solutions are to increase the gap width and to make the metal surfaces within the gap as smooth as possible. As planar traps and planar trap arrays get smaller it will be necessary to investigate these solutions further.

C. Finite boundaries

For laboratory traps it is difficult to approximate an infinite electrode plane and to keep all parts of the apparatus many trap diameters away from the trapping volume. The effects of realistic finite boundary conditions are thus extremely important. For smaller planar Penning traps the finite boundaries may be less important.

One choice of finite boundary conditions comes from locating a planar trap within a grounded conducting cylinder closed with a flat plate (Fig. 12). The boundary conditions in the electrode plane are still given in Fig. 3 for $\rho < \rho_c$. The boundary conditions at infinity in Eq. (6) are replaced by

$$V(\rho_c, z) = 0, \tag{53}$$
$$V(\rho, z_c) = 0. \tag{54}$$

Particles can be loaded into the trap through a hole through the conducting plate above that is small enough to negligibly affect the potential near the particle.

The solution to Laplace's equation for $z > 0$ that satisfies these boundary conditions can be written as

$$V(0, \tilde{z}) = \sum_{i=1}^{N} \Delta V_i \, \Phi_i(\tilde{z}; \tilde{\rho}_c, \tilde{z}_c). \tag{55}$$

Standard electrostatics methods [25,26] give dimensionless potentials,

$$\Phi_i(\tilde{z}; \tilde{\rho}_c, \tilde{z}_c) = \frac{\tilde{\rho}_i}{\tilde{\rho}_c} \sum_{n=1}^{\infty} \frac{2 J_1\left(\alpha_{0n} \frac{\tilde{\rho}_i}{\tilde{\rho}_c}\right)}{\alpha_{0n} J_1^2(\alpha_{0n})} \frac{\sinh\left(\alpha_{0n} \frac{\tilde{z}-\tilde{z}_c}{\tilde{\rho}_c}\right)}{\sinh\left(\alpha_{0n} \frac{\tilde{z}_c}{\tilde{\rho}_c}\right)}, \tag{56}$$

that are functions of zeros of the lowest-order Bessel function, with $J_0(\alpha_{0n}) = 0$. The potential off the axis is given by substituting $V(\tilde{\rho}, \tilde{z})$ for $V(0, \tilde{z})$ in Eq. (55), and inserting $J_0(\alpha_{0n}\tilde{\rho}/\tilde{\rho}_c)$ to the far right in Eq. (56). The planar trap described in Eq. (12) is recovered in the limit of large $\tilde{\rho}_c$ and $\tilde{z}_c$ insofar as the $\Phi_i(\tilde{z}; \tilde{\rho}_c, \tilde{z}_c)$ reduce to the $\Phi_i(\tilde{z})$ of Eq. (13).

The simplest approach is to bias the electrodes of the enclosed trap as if it was an ideal planar trap with no enclosure,
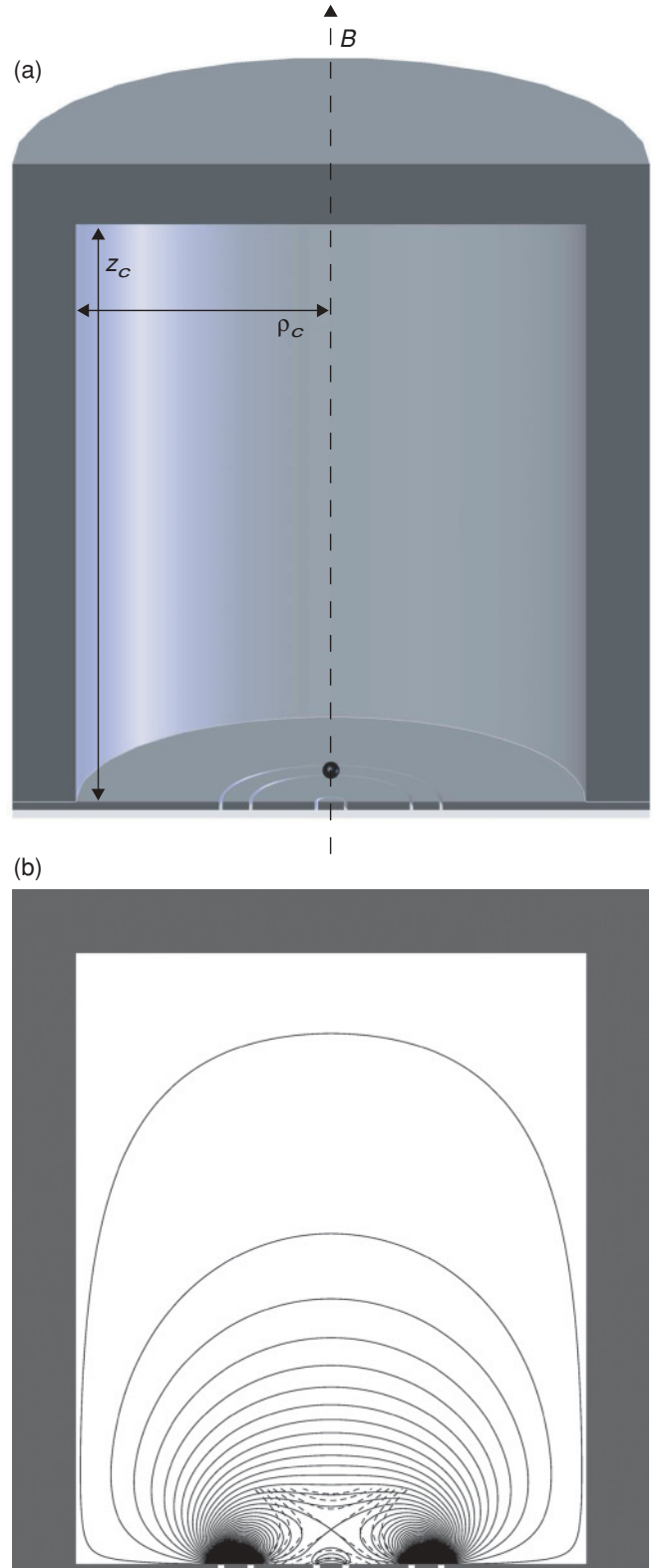
FIG. 12. (a) Planar trap enclosed within a conducting, capped cylinder. Particles can be loaded through a tiny axial hole in the cover (not visible). (b) Side view of trap electrodes and equipotentials spaced by V_0, with the infinitesimal gaps between the electrodes widened to make them visible. The equipotentials extend into the gaps between electrodes. The dashed equipotentials of an ideal quadrupole are superimposed near the trap center.

TABLE V. A conducting enclosure changes the C_k and a_k when the optimal potentials for an ideal planar trap (from Tables I and II) are applied. The enclosure for the sample trap is shown to scale in Fig. 12 with $\rho_c = 19.05$ mm and $z_c = 45.72$ mm.

	$\{\widetilde{\rho}_i\} = \{1, 5.5, 7.5426\}$			
	$a_2 = a_4 = 0$		$C_3 = C_4 = 0$	
	I	II	III	IV
	Eq. (46)	Eqs. (46), (50)	Eqs. (48), (50)	Eq. (48)
$\widetilde{z}_0$	2.2406	1.2750	1.2750	0.8481
C_3	−0.1586	−0.0034	−0.0034	0.0110
C_4	0.0365	0.0082	0.0082	−0.0414
C_5	−0.0193	−0.0081	−0.0081	0.0785
C_6	0.0075	−0.0075	−0.0075	−0.0712
a_2	0.0038	0.0062	0.0062	−0.0312
a_3	−0.0006	0.0000	0.0000	−0.0003
a_4	−0.0003	−0.0072	−0.0072	−0.0701
a_5	0.0001	0.0000	0.0000	−0.0040
a_6	−0.0004	−0.0069	−0.0069	−0.0064
Δf_z @ 5 K	190 Hz	310 Hz	310 Hz	1600 Hz

using the potentials tabulated in Tables I and II. The size of the resulting C_k and a_k coefficients are then displayed in Table V for the conducting enclosure shown to scale in Fig. 12 with dimensions $\rho_c = 19.05$ mm and $z_c = 45.72$ mm, both substantially larger than $\rho_3 = 8$ mm. The resulting thermal frequency shifts for a 5 K axial motion are large enough that this broadening will make it hard to observe one electron and realize a one-electron qubit.

It is possible to do much better by shifting the potentials applied to the trap electrodes, without changing the relative geometry of the electrodes. Table VI shows the required potential shifts and the calculated C_k and a_k that result for each of the four optimized planar trap configurations for an ideal planar trap (summarized in Tables I and II). The frequency broadening is small enough that it should be possible to observe one electron within such a trap.

The configurations in columns II and III of Table VI no longer coincide exactly, however, even though both trap configurations still have very attractive properties. The finite boundary conditions effectively shift the dashed line in Fig. 7 that represents the possible geometries for which an optimized three-gap trap can be realized, so that the relative geometry of the sample trap no longer allows this highest level of optimization. What could be done is to slightly change one of the trap radii to compensate for the calculated effect of the finite boundary conditions. However, the shift of geometry is often less than the size of the typical imprecision with which the electrode radii of a real trap can be fabricated (discussed in the next section) so in practice this makes little sense.

D. Imprecision in trap dimensions and symmetry

A fabricated laboratory trap will not have exactly the intended dimensions and symmetry because of unavoidable fabrication imprecision. Such effects can only be estimated. The simple estimation method used here has proved itself to be adequate for the design of cylindrical traps [16] and open-access traps [20].

TABLE VI. For a conducting enclosure around the sample trap, optimized trap configurations can be obtained by shifting the applied potentials by δV_i and $\delta \widetilde{V}_i$ from the values for an ideal planar trap in Tables I and II. The enclosure for the sample trap is shown to scale in Fig. 12 with $\rho_c = 19.05$ mm and $z_c = 45.72$ mm. Note that configurations II and III are now distinct.

	$\{\widetilde{\rho}_i\} = \{1, 5.5, 7.5426\}$				
	$a_2 = a_4 = 0$		$C_3 = C_4 = 0$		
	I	II	III	IV	
	Eq. (46)	Eqs. (46), (50)	Eqs. (48), (50)	Eq. (48)	
$\delta \widetilde{V}_1$	1.2769	1.4585	1.6122	1.6247	
$\delta \widetilde{V}_2$	1.1724	1.4626	1.6088	1.6239	
$\delta \widetilde{V}_3$	1.9777	2.2179	2.6248	2.5540	
δV_1	−1.3971	−1.5958	−1.7640	−1.7777	V
δV_2	−1.2828	−1.6003	−1.7603	−1.7768	V
δV_3	−2.1639	−2.4267	−2.8719	−2.7944	V
$\widetilde{z}_0$	2.3625	1.4333	1.4436	1.0225	
C_3	−0.1520	0.0013	0.0000	0.0000	
C_4	0.0289	0.0000	0.0000	0.0000	
C_5	−0.0155	−0.0111	−0.0113	0.0220	
C_6	0.0064	0.0000	0.0002	−0.0371	
a_2	0.0000	0.0000	0.0000	0.0000	
a_3	0.0000	0.0000	0.0000	0.0000	
a_4	0.0000	0.0000	0.0002	−0.0347	
a_5	0.0000	0.0000	0.0000	0.0000	
a_6	−0.0003	−0.0039	−0.0038	−0.0095	
Δf_z @ 5 K	0.0	0.0	0.0	0.0	Hz

We start with an achievable fabrication tolerance of 0.001 in = 25 μm that is realistic for existing traps of the size of our sample trap. (Whether smaller traps can be constructed with better fractional tolerances is being investigated [37].) Adding and subtracting the achievable tolerance to the radii ρ_2 and ρ_3 of a three-gap planar trap makes variations (Table VII) from the design ideal (Tables I and II).

These variations do not have the exact ratios of the trap radii needed to make an optimized harmonic trap configuration [Eq. (50)] that is specified by the dashed line in Fig. 7 and in Fig. 10(a). The variations have better properties than what has been observed to date with a laboratory planar trap. However, the imprecision in the radii still makes the predicted broadening of an electron's axial resonance for a 5 K thermal distribution of axial energies to be too large to observe one trapped electron very well. It would be virtually impossible to realize a one-electron qubit.

The solution must be to slightly adjust the potentials on the electrodes to recover properties closer to the ideal, if this is possible. In the cases of the gaps and the conducting enclosure we saw that this could be done, at least in principle, by calculating what the improved set of potentials should be. For imprecision in the trap radii, however, the effective radii for the electrodes will be unknown and hence no such calculation is possible. What is required is a procedure for tuning the potentials of the trap to narrow the thermal broadening. For trap design we must make sure that the trap potentials can be tuned to compensate for imperfections of this order. The tuning procedure and range is the subject of the next section.

TABLE VII. Changes of 0.001 in $= 25\ \mu$m for the electrode radii of the sample trap deteriorate its performance when the potentials for an ideal optimized harmonic configuration (from Tables I and II) are applied.

$\delta\rho_2$	-25	25	0	0	μm
$\delta\rho_3$	0	0	-25	25	μm
$\widetilde{z}_0$	1.4809	1.3876	1.3966	1.4726	
C_3	0.0017	-0.0027	-0.0017	0.0012	
C_4	-0.0036	0.0038	0.0024	-0.0024	
C_5	-0.0108	-0.0112	-0.0111	-0.0110	
C_6	0.0011	-0.0016	-0.0012	0.0009	
a_2	-0.0027	0.0028	0.0018	-0.0018	
a_3	0.0000	0.0000	0.0000	0.0000	
a_4	0.0011	-0.0016	-0.0012	0.0009	
a_5	0.0000	0.0000	0.0000	0.0000	
a_6	-0.0031	-0.0048	-0.0046	-0.0033	
Δf_z @ 5 K	130	140	93	89	Hz

Imperfections that are not cylindrically symmetric are no doubt present. While it is possible with some effort to make calculations of potential configurations that are not cylindrically symmetric [37], the input from imperfections that should be used in such a calculation is difficult to estimate. Fortunately, the experience with earlier traps suggests that this is not necessary for trap design.

E. Tuning a laboratory trap

The point of carefully designing the optimized traps for which the lowest order a_k vanish, preferably along with C_3 and C_4, is not that we actually expect to realize this performance in a real laboratory trap. The previous section illustrates that radius imprecision alone will keep this from happening. The reason for the careful optimized designs is to make sure that imprecision alone will make these crucial coefficients differ from zero. Notice in Table VII that the imperfections considered do not make either a_3 or a_5 deviate much from zero, and a_4 stays at an acceptably low value.

To make a useful trap we need a way to tune the trap *in situ* to make $a_2 = 0$. The other important coefficients will remain small enough because of the optimized design. To tune out the effect of radius imperfections in our sample trap, for example, the trap must be tuned to change the size of a_2 by about ± 0.003. After each adjustment the width of the axial resonance line can be measured to see if the thermal broadening has been reduced or increased.

For the cylindrical Penning trap used to observe one-quantum transitions of one electron, tuning of the trap was essential to the observations that were made. In that trap, like every trap within which precise frequency measurements are made, the effect of imperfections could never be calculated well enough to be useful. *In situ* tuning of a compensation potential was always needed.

For a cylindrical trap, tuning is a straightforward (if a bit tedious) matter. To a good approximation, the potential applied to the compensation electrodes [Fig. 1(c)] changes a_2, while the potential applied between the endcap and ring electrodes

changes V_0 and ω_z. The axial resonance line is measured after every adjustment of the compensation potential to see if the thermal broadening increased or decreased. The "orthogonalized design" of this trap kept the change in the compensation potential from changing the axial frequency very much at all. The axial resonance line was thus easy to keep track of during trap tuning, and the axial oscillation never comes close to going out of resonance with the detection circuit.

The tunability defined in Eq. (32) quantifies how much the axial frequency changes for a given change in a_2 when the potential on a particular electrode is changed. For the compensation electrodes of the cylindrical trap the tunability was 0 for a perfect trap, and $\gamma_{\mathrm{comps}} = 0.03$ was realized for a laboratory trap (Sec. VI B). The much larger $\gamma_{\mathrm{ring}} = -141$ indicates that this electrode is for changing the axial frequency of the trap rather than for tuning a_2.

For a planar Penning trap such an orthogonalization is unfortunately not possible. Changing the potential on each electrode will change both a_2 and ω_z, as indicated by tunabilities in Table I that are not small and which do not vary much from electrode to electrode in most cases (e.g., $|\gamma_i| \approx 3$ in one example). The result is that it is necessary to adjust two or three of the potentials applied to the electrodes of a three-gap trap for each step involved in tuning the trap. Adjustments of the applied potentials must be chosen to vary a_2 by a reasonable amount while keeping V_0 and ω_z fixed.

Figure 13 identifies the potentials for which $a_2 = 0$ and $a_4 = 0$ for our sample trap with and without the radius imperfections of Table VII. For each point on this plot V_1 has been adjusted so that V_0 and hence the axial frequency ω_z remain fixed. In this example it would be necessary to change V_2 or V_3 (along with V_1 to keep V_0 fixed) to achieve $a_2 = 0$.
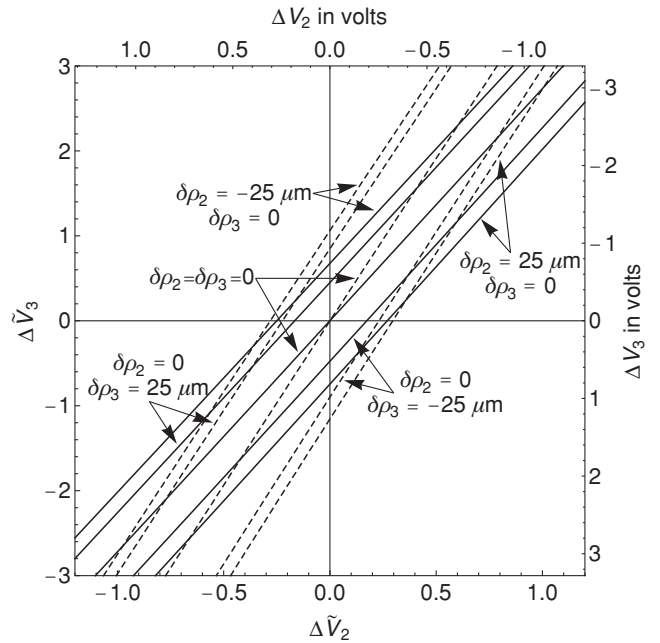

FIG. 13. The $a_2 = 0$ (solid) and $a_4 = 0$ (dashed) contours for the sample trap with one of its radii displaced by the indicated distance as a function of the potentials applied to the electrodes. V_2 and V_3 are changed as plotted, and V_1 is adjusted to keep the axial frequency at 64 MHz.
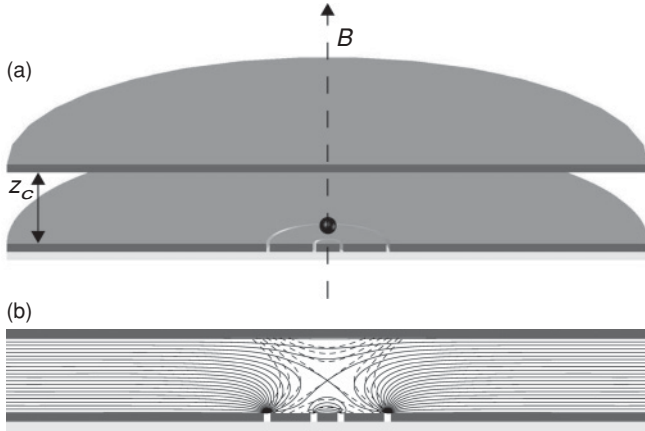
FIG. 14. (a) A covered planar Penning trap could be loaded through a tiny axial hole in the cover (not visible). (b) Side view of trap electrodes and equipotentials spaced by V_0, with the infinitesimal gaps between the electrodes widened to make them visible. Some equipotentials extend into the gaps between electrodes and some terminate at infinity. The dashed equipotentials of an ideal quadrupole are superimposed near the trap center.

However, by changing both V_2 and V_3 (along with V_1) it would be possible to make $a_2 = 0$ while at the same time making a_4 much smaller in magnitude.

VIII. COVERS AND MIRRORS

A. Covered planar trap

A covered planar Penning trap (Fig. 14) is a planar trap that is electrically shielded by a nearby conducting plane. The covered planar trap has some very attractive features.

1. The electrodes are in a single plane that can be fabricated as part of a single chip.

2. The conducting plane provides an easily controlled boundary condition above the electrode plane that needs no special fabrication, nor any alignment beyond making the planes parallel.

3. A trap that is radially infinite is well approximated if the radial extent of the two planes beyond the electrodes is large compared to their spacing.

4. A covered planar trap is naturally scalable to an array of traps.

5. The axial motion of electrons in more than one trap could be simultaneously detected with a common detection circuit attached to the cover.

6. The axial motions of electrons in more than one trap could be coupled and uncoupled as they induce currents across a common detection resistor by tuning the axial motions of particular electrons into and out of resonance with each other.

Three possible additional advantages emerge when the properties of the trapping potential in a covered planar trap are considered.

1. A two-gap covered planar trap can be optimized in much the same way as a three-gap infinite planar trap.

2. Smaller gap potentials can sometimes be used to achieve optimized configurations, permitting smaller gap widths and better screening of the exposed insulator between electrodes.

3. In some cases a smaller a_6 can be realized for trap configurations with $a_2 = a_3 = a_4 = a_5 = 0$.

These possibilities are illustrated using an example.

The secondary advantages for planar Penning traps (mentioned in the Introduction) may be diminished when a cover is used. Microwaves of small wavelength can be introduced between the electrode plane and the cover. However, the added complication of small striplines [38] is likely required for longer wavelengths. It should not be significantly more difficult to load electrons with typical methods via small holes in the electrodes, but if other loading mechanisms are used then the electron trajectories may be obstructed by the cover.

The potential between the electrode plane and the cover plane is a superposition of terms proportional to the potentials applied to the electrodes, V_i, and the potential applied to the cover plane, V_c,

$$V(0, \tilde{z}) = \sum_{i=1}^{N} \Delta V_i \Phi_i(\tilde{z}; \tilde{z}_c) + V_c \Phi_c(\tilde{z}; \tilde{z}_c). \quad (57)$$

The grounded cover plane makes the $\Phi_i(\tilde{z})$ of Eq. (13) dependent upon $\tilde{z}_c$,

$$\Phi_i(\tilde{z}; \tilde{z}_c) = \tilde{\rho}_i \int_0^\infty dk \frac{\sinh[k(\tilde{z} - \tilde{z}_c)]}{\sinh(k\tilde{z}_c)} J_1(k\tilde{\rho}_i), \quad (58)$$

which approaches $\Phi_i(\tilde{z})$ for large $\tilde{z}_c$. Biasing the cover plane at a nonvanishing V_c superimposes a uniform electric field, described by

$$\Phi_c(\tilde{z}; \tilde{z}_c) = \tilde{z}/\tilde{z}_c, \quad (59)$$

between the large electrode and cover planes.

The scaled geometry and potentials of a two-gap covered planar Penning trap are characterized by six parameters ($\tilde{\rho}_2$, $\tilde{z}_c$, $\tilde{V}_1$, $\tilde{V}_2$, $\tilde{V}_c$, and $\tilde{z}_o$). This is the same number of parameters that characterize a three-gap planar trap with no cover electrode, the optimization of which was discussed in detail in Sec. VI.

The trap geometries that can be optimized are represented in Fig. 15. The six parameters can be chosen to satisfy the same sets of four constraints considered in Sec. VI, giving the various shaded regions in Fig. 15. The six parameters can be chosen to satisfy the five constraints of Eq. (50) on the dashed curve in Fig. 15 for which $C_3 = C_4 = C_6 = a_2 = a_3 = a_4 = a_5 = 0$.

The optimized harmonic configuration represented by the dot in Fig. 15 has its scaled parameters listed in Table VIII. One set of possible absolute parameters is listed in Table IX. In the following section we discuss other attractive features of this particular configuration.

Figure 14(b) shows equipotentials spaced by V_0 for a covered planar Penning trap (configuration I in Table VIII). The equipotentials are calculated for infinitesimal gaps, but the electrodes are represented with finite gaps to make them visible. The equipotentials terminate in the gaps between electrodes or at infinity. The dashed equipotentials of an ideal quadrupole are superimposed near the trap center.

Covered planar traps are scalable in that an array of traps can share the same covering plane at potential V_c, with the axial frequency and the harmonic properties of each trap being tuned by the potentials applied to the other electrodes. This is analogous to Fig. 13 in which a_2 can be tuned at constant frequency by changing only V_1 and V_2 while leaving V_3 fixed.
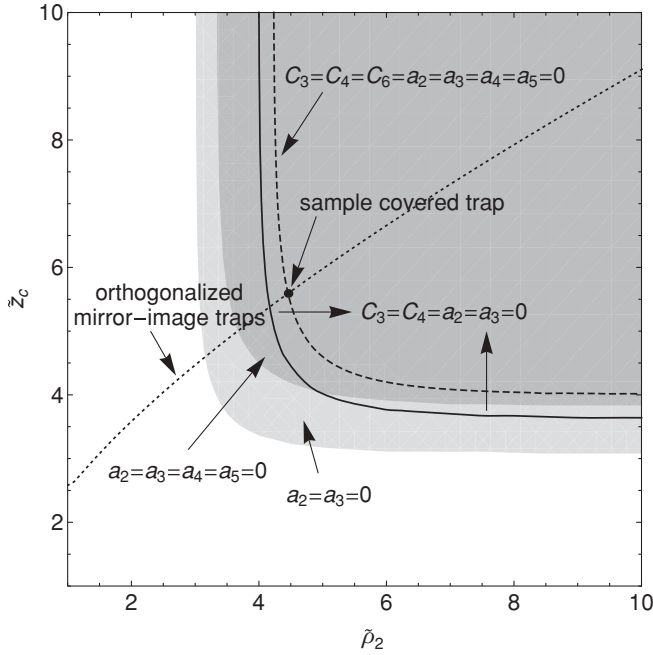
FIG. 15. Parameter space regions for which the indicated a_k can be made to vanish for a two-gap planar trap with a cover, along with the region and the curve for which the indicated C_k can alternatively be made to vanish. No optimized traps are possible in the unshaded region. The dotted line indicates orthogonalized mirror-image traps formed from two sets of two-gap planar trap electrodes, as described in Sec. VIII B.

TABLE VIII. Scaled parameters for the sample two-gap covered planar trap geometry.

	$\{\widetilde{\rho}_i\} = \{1, 4.4572\}, \tilde{z}_c = 5.5914$			
	$a_2 = a_4 = 0$		$C_3 = C_4 = 0$	
	I	II	III	IV
	Eq. (46)	Eqs. (46), (50)	Eqs. (48), (50)	Eq. (48)
$\widetilde{V}_1$	23.6322	23.9786	23.9786	24.2851
$\widetilde{V}_2$	19.0275	23.3251	23.3251	23.6609
$\widetilde{V}_c$	21.2413	29.8478	29.8478	32.4943
$\tilde{z}_0$	2.4214	1.4338	1.4338	1.0306
C_3	−0.1532	0.0000	0.0000	0.0000
C_4	0.0294	0.0000	0.0000	0.0000
C_5	−0.0143	−0.0099	−0.0099	0.0208
C_6	0.0057	0.0000	0.0000	−0.0351
a_2	0.0000	0.0000	0.0000	0.0000
a_3	0.0000	0.0000	0.0000	0.0000
a_4	0.0000	0.0000	0.0000	−0.0329
a_5	0.0000	0.0000	0.0000	0.0000
a_6	−0.0003	−0.0038	−0.0038	−0.0096
C_{11}	−0.1155	−0.3781	−0.3781	−0.6789
C_{12}	−0.2558	−0.0690	−0.0690	0.2056
C_{1c}	0.3577	0.3577	0.3577	0.3577
$C_{1d}^{(opt)}$	−0.3715	−0.5521	−0.5521	−0.7545
γ_1	−142.78	3.37	3.37	3.47
γ_2	6.72	2.34	2.34	4.28
γ_c	7.64	0.00	0.00	0.00

The effect of a grounded radial boundary at $\tilde{\rho}_c$ (rather than at infinity) can also be calculated. The superposition

$$V(0, \tilde{z}) = \sum_{i=1}^{N} \Delta V_i \Phi_i(\tilde{z}; \tilde{\rho}_c, \tilde{z}_c) + V_c \Phi_c(\tilde{z}; \tilde{\rho}_c, \tilde{z}_c), \quad (60)$$

has dimensionless potentials that depend upon the distance to the radial boundary, $\tilde{\rho}_c$, as well as upon $\tilde{z}_c$. The first of these,

$$\Phi_i(\tilde{z}; \tilde{\rho}_c, \tilde{z}_c) = \frac{\tilde{\rho}_i}{\tilde{\rho}_c} \sum_{n=1}^{\infty} \frac{2 J_1\left(\alpha_{0n} \frac{\tilde{\rho}_i}{\tilde{\rho}_c}\right)}{\alpha_{0n} J_1^2(\alpha_{0n})} \frac{\sinh\left(\alpha_{0n} \frac{\tilde{z}-\tilde{z}_c}{\tilde{\rho}_c}\right)}{\sinh\left(\alpha_{0n} \frac{\tilde{z}_c}{\tilde{\rho}_c}\right)}, \quad (56)$$

was used earlier in Eq. (56) to describe a grounded enclosure around a planar trap. The second,

$$\Phi_c(\tilde{z}; \tilde{\rho}_c, \tilde{z}_c) = \sum_{n=1}^{\infty} \frac{2}{\alpha_{0n} J_1(\alpha_{0n})} \frac{\sinh\left(\alpha_{0n} \frac{\tilde{z}}{\tilde{\rho}_c}\right)}{\sinh\left(\alpha_{0n} \frac{\tilde{z}_c}{\tilde{\rho}_c}\right)}, \quad (61)$$

goes to the uniform field limit of Eq. (59) in the limit of large $\tilde{\rho}_c$. These potentials can be used to investigate radial boundary effects as needed, though we will not give examples here.

B. Mirror-image trap

A mirror-image planar trap (Fig. 16) is a set of two planar electrodes that are biased identically and face each other. The axial potential,

$$V(0, \tilde{z}) = \sum_{i=1}^{N} \Delta V_i \left[\Phi_i(\tilde{z}; \tilde{z}_c) + \Phi_i(\tilde{z}_c - \tilde{z}; \tilde{z}_c) \right], \quad (62)$$

is a function of the dimensionless potentials defined in Eq. (56).

For a two-gap mirror-image trap there are only four scaled parameters to be chosen ($\tilde{\rho}_2, \tilde{z}_c, \widetilde{V}_1, \widetilde{V}_2$). The mirror-image symmetry of the electrodes ensures that the potential minimum is midway between the electrode planes and that all odd-order C_k vanish. The constraints are $C_2 = 1$, $C_4 = 0$, and $C_{22} = 0$, the latter giving the orthogonality property discussed in the following. With one more parameter than constraints, the

TABLE IX. A set of absolute values for the sample two-gap covered planar trap geometry.

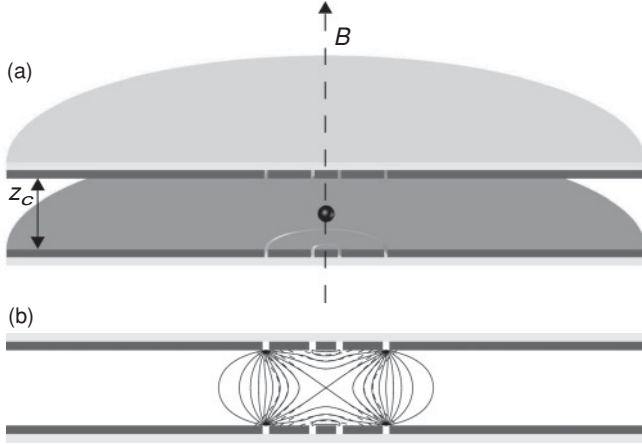|					
	$\{\rho_i\} = \{1, 4.4572\}$ mm, $z_c = 5.5914$ mm				
	$a_2 = a_4 = 0$		$C_3 = C_4 = 0$		
	I	II	III	IV	
	Eq. (46)	Eqs. (46), (50)	Eqs. (48), (50)	Eq. (48)	
ρ_1	1	1	1	1	mm
z_0	2.4214	1.4338	1.4338	1.0306	mm
$\rho_d^{(opt)}$	4.6396	2.1166	2.1166	1.4797	mm
f_z	64	64	64	64	MHz
V_0	−0.9194	−0.9194	−0.9194	−0.9194	V
V_1	−21.7271	−22.0456	−22.0456	−22.3274	V
V_2	−17.4936	−21.4448	−21.4448	−21.7535	V
V_c	−19.5290	−27.4416	−27.4416	−29.8749	V
Δf_z	0.0	0.0	0.0	0.0	Hz
$1 : \gamma_z$	2π 1.50	2π 16.03	2π 16.03	2π 51.68	s^{-1}
$2 : \gamma_z$	2π 7.34	2π 0.53	2π 0.53	2π 4.74	s^{-1}
$c : \gamma_z$	2π 14.35	2π 14.35	2π 14.35	2π 14.35	s^{-1}
$d : \gamma_z^{(opt)}$	2π 15.47	2π 34.18	2π 34.18	2π 63.83	s^{-1}

FIG. 16. (a) A mirror-image Penning trap is formed with two planar trap electrodes facing each other. Particles can be loaded through a tiny axial hole in one of the electrodes (not visible). (b) Side view of trap electrodes and equipotentials spaced by V_0, with the infinitesimal gaps between the electrodes widened to make them visible. The equipotentials extend into the gaps between electrodes. The dashed equipotentials of an ideal quadrupole are superimposed near the trap center.

possible geometries for a two-gap mirror-image trap are given by the dotted curve in Fig. 15. The filled circle on this curve represents the trap geometry that is used to illustrate the properties of a mirror-image trap in Fig. 16 and in Tables X and XI.

The properties of a mirror-image trap are similar to those of the cylindrical Penning trap [Fig. 1(c)] used to suspend one

TABLE X. Scaled parameters for the sample two-gap mirror-image planar trap geometry.

$\{\widetilde{\rho}_i\} = \{1, 4.4572\}, \bar{z}_c = 5.5914$	
$C_3 = C_4 = 0$, Eq. (48)	
$\widetilde{V}_1 = \widetilde{V}_1^{\text{top}}$	13.9582
$\widetilde{V}_2 = \widetilde{V}_2^{\text{top}}$	12.3743
$\widetilde{V}_3 = \widetilde{V}_3^{\text{top}}$	0.0000
$\widetilde{z}_0$	2.7957
C_3	0.0000
C_4	0.0000
C_5	0.0000
C_6	0.0015
a_2	0.0000
a_3	0.0000
a_4	0.0014
a_5	0.0000
a_6	0.0002
$C_{11} = -C_{11}^{\text{top}}$	−0.0811
$C_{12} = -C_{12}^{\text{top}}$	−0.2624
$C_{13} = -C_{13}^{\text{top}}$	−0.0142
$C_{1d}^{\text{(opt)}}$	−0.3577
$\tilde{\rho}_d^{\text{(opt)}}$	∞
$\gamma_1 = \gamma_1^{\text{top}}$	4.35
$\gamma_2 = \gamma_2^{\text{top}}$	0.00
$\gamma_3 = \gamma_3^{\text{top}}$	−33.96

TABLE XI. A set of absolute values for the sample two-gap mirror-image planar trap geometry.

$\{\widetilde{\rho}_i\} = \{1, 4.4572\}, \bar{z}_c = 5.5914$		
$C_3 = C_4 = 0$, Eq. (48)		
ρ_1	1	mm
z_0	2.7957	mm
$\rho_d^{\|\text{opt}\|}$	∞	mm
f_z	64	MHz
V_0	−0.9194	V
$V_1 = V_1^{\text{top}}$	−12.8330	V
$V_2 = V_2^{\text{top}}$	−11.3768	V
$V_3 = V_3^{\text{top}}$	0.0000	V
Δf_z	0.0	Hz
$1 : \gamma_z$	$2\pi\ 0.74$	s^{-1}
$2 : \gamma_z$	$2\pi\ 7.72$	s^{-1}
$3 : \gamma_z$	$2\pi\ 0.02$	s^{-1}
$d : \gamma_z^{\text{(opt)}}$	$2\pi\ 14.35$	s^{-1}

electron and to observe its one-quantum cyclotron transitions and spin flips. A charged particle suspended midway between the two electrode planes sees a potential that is symmetric under reflections across this midplane, in which case all odd-order potential coefficients (C_3, C_5, etc.) vanish, as for the cylindrical trap (Sec. VI B). Also, as for a cylindrical trap, we can choose the potentials applied to the trap electrodes to make a trap with a very small C_4, whereupon a_2 and a_3 are very small.

A useful property of mirror-image traps and cylindrical traps is that both of these can be "orthogonalized" in a way that a planar trap cannot. A single potential (applied to two electrodes with mirror-image symmetry) is tuned to minimize the amplitude-dependence of the axial frequency. The trap is orthogonalized in that this tuning does not change the axial frequency, which in general would take it out of resonance with the detection circuit.

Figure 16(b) shows equipotentials spaced by V_0 for the mirror image Penning trap of Table X. The equipotentials are calculated for infinitesimal gaps, but the electrodes are represented with finite gaps to make them visible. The equipotentials terminate in the gaps between electrodes. The dashed equipotentials of an ideal quadrupole are superimposed near the trap center.

C. Mirror-image trap transformed to a covered trap

At least for initial studies it may be useful first to load an electron into the center of an orthogonalized mirror-image trap. The presence of a single electron can be established with established methods used with cylindrical Penning traps. The challenge is then to adiabatically change the potentials applied to the electrodes to turn the mirror-image trap into a covered planar trap. It is crucial that the electron not be lost. If a high quality trapping well can be maintained throughout the transfer, then it may even be possible to monitor the electron at intermediate points between the two configurations.

We investigate the feasibility of transferring from the mirror-image trap discussed above (Tables X and XI) to the optimized, covered planar trap discussed in the last section (Tables VIII and IX). The electrode geometry chosen for our
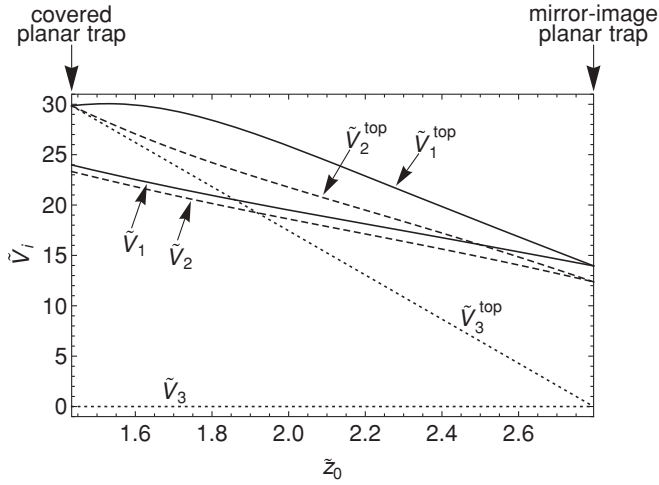
FIG. 17. One set of applied potentials that relocates an electron centered between the electrode planes of a mirror-image planar trap (far right) to a covered planar trap (far left) while keeping the axial frequency constant and keeping $a_2 = a_3 = C_3 = C_4 = 0$.

example is the lone point in Fig. 15 for which it is possible to make an orthogonalized mirror-image trap and also to make a the most highly optimized covered planar Penning trap. The potentials applied to achieve the mirror-image trap are those to the far right in Fig. 17. The potentials applied to realize the covered planar trap are those to the far left in Fig. 17.

For these traps there are six parameters to choose: five relative trap potentials ($\widetilde{V}_1$, $\widetilde{V}_2$, $\widetilde{V}_1^{top}$, $\widetilde{V}_2^{top}$, $\widetilde{V}_3^{top}$) and $\tilde{z}_0$. During the transfer we can choose a particular $\tilde{z}_0$ as a constraint, along with four others that we have discussed earlier, $C_1 = C_3 = C_4 = 0$ and $C_2 = 1$. Since there are more parameters than constraints there is some freedom in the choice of potentials during the transfer, provided that solutions exist. Our choice of intermediate potentials in Fig. 17 was made to avoid large potential differences between electrodes (discussed in Sec. VII B). The axial oscillation frequency does not change during the transfer. Also, the trap remains optimized during every point in the transfer, with $a_2 = a_3 = C_3 = C_4 = 0$. It may thus be possible to detect the electron's axial oscillation at every step of the transfer.

IX. DAMPING AND DETECTING AN AXIAL OSCILLATION

A. Damping and detection in a planar trap

The damping rate γ_z for the axial motion of a trapped particle is the observed resonance linewidth for the axial motion in the limit of a vanishing oscillation amplitude. A thermal distribution of axial oscillation amplitudes broadens the observed resonance linewidth when the axial frequency is amplitude dependent. When the oscillation energy has Fourier components that extend well beyond the damping linewidth, it is difficult to detect the oscillation with the narrow-band detection methods needed to observe the small signal from a single particle. For the cylindrical Penning trap used to observe one-quantum transitions of a single trapped electron [1] this was not a problem. The thermal anharmonicity contribution to the linewidth was less than the damping linewidth. For the Ulm

planar trap the situation was very different. The thermal width was 10^5 times larger than the damping linewidth, making it impossible to observe a single electron at all [13].

In preceding sections we focused upon minimizing the amplitude-dependence of the axial frequency so that the thermal broadening could be reduced. Just as important is increasing the axial damping linewidth. Here we discuss what is needed to maximize the electron's damping rate. Maximizing the damping maximizes the detected signal as well.

The usual method to probe the axial oscillation of a single trapped particle is to detect the current that its axial motion induces in a resistor R connected to its electrodes [31,39]. This resistance also damps the motion. The energy dissipated in the resistor comes from the axial motion of the trapped particle, which is thereby damped to the bottom of the axial potential well. In practice the resistor is a tuned circuit that is resonant at the axial oscillation frequency, at which frequency it acts as a pure resistance.

For a planar Penning trap, Fig. 18 illustrates how the AC connections between the circuit and the electrodes can be made to the same electrodes that are DC biased to form the trapping potential. Alternatively, an extra gap (e.g., the dashed circle labeled ρ_d in Fig. 18) can be added to one of the trap's electrodes to maximize the damping and detection, as will be discussed. This damping-detection gap can coincide with one of the gaps already chosen to minimize the amplitude-dependence of the axial frequency. When the extra gap does not coincide with one of the others, the extra gap will not change the electrostatic trapping potential insofar as the same DC bias voltage is applied to either side of the additional gap.

The circuit in Fig. 18 represents one way to connect the detection and damping resistance, R, to the electrodes of a three-gap planar trap. The current induced by the particle's axial oscillation makes an instantaneous voltage V_I across the resistance. This induced voltage exerts a reaction force on the trapped particle. The thermal Johnson noise from random electron motions within the resistor induces an additional instantaneous noise voltage V_n across the resistor and electrodes. The oscillatory voltage $V_I + V_n$ on the effective damping
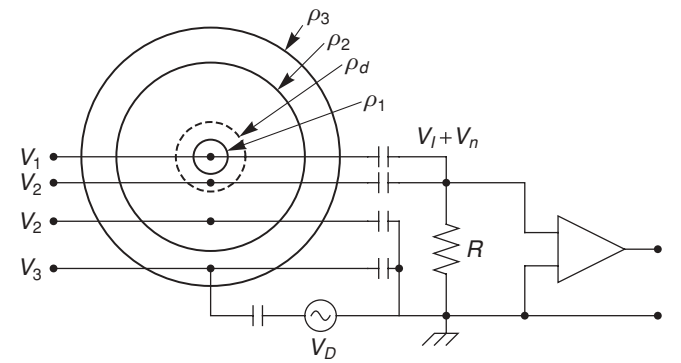

FIG. 18. Electrical circuit used to bias, detect, damp, and drive a trapped particle's axial motion. An extra gap (dashed circle) in the electrodes of the planar trap can be added to optimize the damping and detection without changing the electrostatic properties of an optimized planar trap. The relative trap geometry is that of the sample trap.

electrode for which $\rho < \rho_d$ both drives the particle's axial motion and is detected.

The particle is in the near field of the potential

$$V_{\mathrm{osc}} = (V_I + V_n)\phi_d, \tag{63}$$

produced by this oscillatory voltage, where the electrostatic potential

$$\phi_d(\tilde{z}) = 1 - \frac{\tilde{z}}{\sqrt{(\tilde{\rho}_d)^2 + \tilde{z}^2}}, \tag{64}$$

follows from Eq. (11).

For a potential V_i applied to electrode i, the instantaneous electric field on a particle oscillating near its equilibrium position at $\tilde{z} = \tilde{z}_0$ is

$$E_i(\tilde{z}_0) \approx -\frac{D_1}{2\rho_1} V_i. \tag{65}$$

The factor D_1 depends upon electrodes to which a voltage is applied to make the field. For a voltage applied just to the damping and detection electrode,

$$D_1 = C_{1d} = \frac{-2(\tilde{\rho}_d)^2}{[(\tilde{z}_0)^2 + (\tilde{\rho}_d)^2]^{3/2}}, \tag{66}$$

where the potential expansion coefficient C_{1i} is defined in Eqs. (14) and (15).

There is a maximum coupling of the circuit and a trapped particle insofar as C_{1d} has a maximum magnitude at

$$\rho_d = \sqrt{2}\tilde{z}_0. \tag{67}$$

The coupling coefficient is then given by

$$C_{1d}^{(\mathrm{opt})} = \frac{-4 \times 3^{-3/2}}{\tilde{z}_0} \approx \frac{-0.77}{\tilde{z}_0}. \tag{68}$$

Figure 19(a) illustrates the maximum for all values of $\tilde{z}_0$.

If instead the electrodes of the optimized planar trap are attached to the resistance, without adding an extra gap at ρ_d, then D_1 is the sum of the C_{1i} for the electrodes attached to the resistor. If the central two electrodes are attached to the detection circuit, for example, then $D_1 = C_{11} + C_{12}$. The coefficients C_{1i} for the optimized configurations of our sample trap are listed in Table I, as is $C_{1d}^{(\mathrm{opt})}$. Figure 19(b) shows how the various possibilities for these coefficients and sums depend upon $\tilde{z}_0$.

The induced signal,

$$V_I = \frac{q D_1}{2\rho_1} R\dot{z}, \tag{69}$$

is proportional to the axial velocity of the oscillating particle, as well as to D_1 and R [31]. The damping force that arises from this induced potential produces the damping rate for a particle of charge q and mass m,

$$\gamma_z = \left(\frac{q D_1}{2\rho_1}\right)^2 \frac{R}{m}, \tag{70}$$

that goes as the square of D_1 [31]. One power of D_1 arises because the induced current is proportional to D_1. The second power arises because a potential on the electrodes induces a damping force that is also proportional to D_1. The damping rates for a resistor connected between a single electrode and ground are listed in Table II for $R = 100$ kΩ. The maximum damping rate $\gamma_z^{(\mathrm{opt})}$ that pertains for Eq. (67) is also tabulated for comparison. As noted previously, if the resistor is connected to more than one electrode then the appropriate
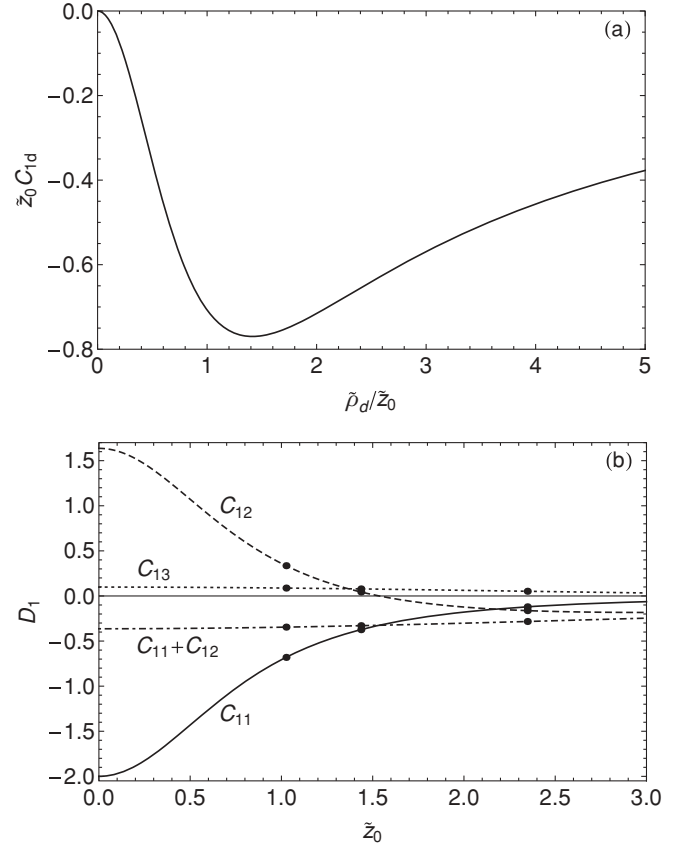

FIG. 19. (a) The coefficient C_{1d} that describes the coupling, and the plotted product $\tilde{z}_0 C_{1d}$, both have a maximum magnitude at $\tilde{\rho}_d = \sqrt{2}\tilde{z}_0$. (b) Electric field coefficients that describe the damping rates and detection efficiency for the sample trap.

coefficients C_{1i} for the connected electrodes must be summed to make D_1 before squaring.

The thermal Johnson noise in the resistor drives a particle that is near to its equilibrium location with a driving force

$$F_n \approx \frac{q D_1}{2\rho_1} V_n. \tag{71}$$

For the circuit shown in Fig. 18 we have $D_1 = C_{1d}$.

An external driving force may be added to drive the axial motion of a trapped particle. Such a driving force has the advantage that a larger oscillation amplitude and hence a larger induced signal is produced at just the frequency of the drive in the steady state. A larger oscillation amplitude, of course, makes it more important to minimize the amplitude-dependence of the axial frequency. One choice is to apply an oscillatory driving voltage V_D to the third electrode, between ρ_2 and ρ_3, as indicated in Fig. 18. The applied driving potential, V_D, produces a driving force on a particle near its equilibrium location that is given by

$$F_D \approx \frac{q D_1}{2\rho_1} V_D. \tag{72}$$

For V_D applied to the third electrode we have $D_1 = C_{13}$.

B. Damping and detection in a covered trap

For a covered planar trap, the damping and the detected signal is maximized by introducing an extra gap at radius

ρ_d and connecting the damping resistor to each of the electrodes with radius $\rho \leqslant \rho_d$. The choice $\rho_d^{(\mathrm{opt})}$ that gives the maximum damping and detection signal, along with the corresponding $C_{1d}^{(\mathrm{opt})}$ and $\gamma_z^{(\mathrm{opt})}$, are displayed in Tables VIII and IX. This detection configuration offers an appreciable detection efficiency. For some achievable values of z_0 the detection efficiency is nearly maximized without the need to make an extra gap in the electrode plane.

As mentioned earlier, covered planar traps are scalable in that an array of traps can share the same covering plane, with the axial frequency and the harmonic properties of each trap being tuned separately by the potentials applied to the other electrodes. Multiple traps can also share the same detection circuit if the detection resistor is attached to the covering plane—a great simplification in practice. Many trapped electrons could be simultaneously detected with one circuit if their axial frequencies are tuned to be slightly different but within the detector's bandwidth. A coupling between two electrons takes place during the time that their two traps are tuned to make their axial frequencies the same.

C. Damping and detection in a mirror-image trap

For a mirror-image trap, the damping and hence the signal is maximized by connecting all of the electrodes in one plane to the damping resistor [i.e., $\rho_d^{(\mathrm{opt})} \to \infty$]. Choosing $\rho_d = z_c/2$ gives γ_z that is 64% of the total possible damping. Choosing $\rho_d = z_c$ gives γ_z that is 98% of the total possible damping. For the sample mirror-image planar trap (Tables X and XI), connecting the damping resistor to the first two electrodes of one of the planes (i.e., choosing $\tilde{\rho}_d = \tilde{\rho}_2$) results in $\gamma_z = 2\pi\,13.23\ \mathrm{s}^{-1}$, which is 92% of the damping that would result from detecting the signal induced on the entire electrode plane.

X. CONCLUSION

A cylindrical Penning trap has been used to observe one-quantum spin flip and cyclotron transitions of a single trapped electron. Attempts to make similar observations in a planar Penning trap did not succeed, generating some pessimism about whether this is possible. In this report we show how to optimize the properties of a planar Penning trap to reduce the deadly amplitude dependence of the monitored axial frequency by orders of magnitude, and how to optimize the damping and detection. We introduce a covered planar trap that is well isolated from its environment, readily scalable to an array of one-electron traps, with one detector promising to suffice for the efficient simultaneous detection of multiple particles. We also introduce mirror-image planar traps that are an attractive option because of their reflection symmetry. A mirror-image trap can be electrically transformed into a covered planar trap while a particle is stored within. The optimized planar trap designs that are proposed offer new routes toward observing a single electron in a planar trap, realizing a one-electron qubit, and using a scalable array of such qubits for quantum information studies.

ACKNOWLEDGMENTS

APPENDIX A: AN EARLIER CALCULATION

Minimizing the amplitude dependence of the axial frequency is the key to designing a planar trap within which a single electron can be suspended and used to realize a one-electron qubit. An accurate description and prediction of the properties of a planar Penning trap configuration thus requires a calculation of the amplitude dependence of the axial frequency. Here we correct an earlier calculation [10] of the amplitude dependent frequency shifts.

Earlier in this work the amplitude dependence of the axial frequency was shown to have the form

$$\omega_z(\widetilde{A}) = \omega_z\left[1 + \sum_{k=2}^{\infty} a_k \widetilde{A}^k\right]. \tag{24}$$

Reference [10] differs by starting this sum with $k = 1$, suggesting that the dominant axial frequency shift is first-order in the oscillation amplitude. We find no first-order shift. The substantial disagreement between the a_k in Eq. (25) with the much simpler

$$a_k = \left|\frac{C_{k+2}}{2}\right|, \tag{A1}$$

from Ref. [10] (translated into our notation) is illustrated in Table XII. The differing expressions for a_3, for example, are not even functions of the same C_k. Higher order a_k differ more. (Eq. (2) of Ref. [11] and also Ref. [12] repeat the Ref. [10] results.)

The amplitude dependence of the axial frequency must be calculated by solving the equation of motion, Eq. (22), to get the a_k in Eq. (25), as outlined between these two equations. Except for the absolute value whose origin is not clear, Eq. (A1) from Ref. [10] is instead consistent with equating $(1/2)m\omega_z^2(z - z_0)^2$ to $q[V(0, z) - V(0, z_0)]$, solving for ω_z, expanding the square root in $z - z_0$, and identifying the latter with A.

Finally, the relationship between energy and amplitude in Eq. (11) of Ref. [10], repeated in Eq. (3) of Ref. [11], is missing a factor of two. It should read $A = \sqrt{2E/(m\omega_z^2)}$.

TABLE XII. Lowest-order coefficients that describe the amplitude dependence of the axial frequency. This work and Ref. [10] differ considerably in amplitude and sign, most notably in the leading lowest order.

This work	Ref. [10]
$a_1 = 0$	$a_1 = \frac{|C_3|}{2}$
$a_2 = -\frac{15(C_3)^2}{16} + \frac{3C_4}{4}$	$a_2 = \frac{|C_4|}{2}$
$a_3 = -\frac{15(C_3)^3}{16} + \frac{3C_3C_4}{4}$	$a_3 = \frac{|C_5|}{2}$

APPENDIX B: MAINZ TRAP

The first planar Penning trap used to store electrons was demonstrated at Mainz [11,12]. A large number of electrons (estimated to be between 100 and 1000 electrons) were stored and the three motions of the electrons' center of mass were observed. The trap dimensions and potentials are given by

$$\rho_i = \{3.15, 6.3, 9.45\} \text{ mm}, \tag{B1}$$

$$V_i = \{0, 16, -38.5\} \text{ V}, \tag{B2}$$

with radii taken to extend to the center of the 0.3 mm wide gaps between electrodes. The potentials come from the caption of Fig. 8 of Ref. [11], but with signs reversed compared to what is reported since this is necessary to approximately replicate the curves in Fig. 8 of that work. Finite boundaries are not included in our analysis, even though Sec. VII C illustrates that they can be important, because the needed information is not available in the experimental accounts.

We calculate that $V_3 = -36.2$ V would make $C_3 = 0$, which seems to have been the goal, whereupon $a_2 = -0.8$ and $C_4 = -1.0$. This gives a calculated single-particle thermal frequency width of $\Delta f_z = 310$ kHz for $T_z = 300$ K. This thermal width is smaller than the calculated and measured widths of 1–6 MHz reported in Fig. 7 of Ref. [11]. Unless the calculation is corrected as described in Appendix A, the calculated width should not agree with what we calculate. The measured width may be wider than expected because there are more trapped electrons than was estimated. Experimental experience in our laboratory also suggests that it is likely that the observed width is broadened by charges accumulated on the insulator within the gaps, since the gaps were not deep enough to screen the potential from such charges.

A minimal requirement for a trap that could be used to observe a single electron is that a_2 be close to zero. Figure 7 shows that for the relative geometry used in the Mainz trap there is no set of applied potentials that could make $a_2 = 0$. In fact, $|a_2| < 0.1$ cannot be achieved for any reasonable values of V_i and z_0. This is true even if the artificial and unnecessary constraint $V_1 = 0$ is relaxed.

APPENDIX C: ULM TRAP

The serious effort made at Ulm to try to observed a single electron trapped in a planar Penning trap [13] did not succeed. Given that we conclude above that optimized planar traps could likely be used to observe one trapped electron, we examine here the trap geometry and the applied potentials that were used. The object is to check whether the performance of the Ulm trap is consistent with our calculations. Given that the observed linewidth is broader than calculated, we also discuss some practical considerations that may have affected the performance.

The trap geometry is described in Sec. 2.1 of Ref. [13]: "The diameter of the central electrode and the width of the trapping electrodes are equal to 2 mm." In our notation, this is

$$\{\rho_1, \rho_2, \rho_3\} = \{1, 3, 5\} \text{ mm}. \tag{C1}$$

Several bias configurations are mentioned in Sec. 2.2 and Fig. 2 of Ref. [13]

$$\{V_1, V_2, V_3\} = \{0, 7, 7\} \text{ V}, \tag{C2}$$

$$\{V_1, V_2, V_3\} = \{0, 5.2, 14\} \text{ V}, \tag{C3}$$

$$\{V_1, V_2, V_3\} = \{0, 4.8, 14\} \text{ V}. \tag{C4}$$

The penultimate paragraph of Sec. 2.3 of Ref. [13] mentions a set of "optimized control voltages",

$$\{V_1, V_2, V_3\} = \{0, -1, 2.611\} \text{ V}, \tag{C5}$$

presumably for the same geometry. However, this last set of potentials seems not to have been used successfully, perhaps because of the greatly reduced trap depth that is produced.

The calculated properties for each of these four configurations are summarized in Tables XIII and XIV. None of these trap configurations make a_2 close to zero, the likely minimal requirement for observing and controlling one trapped electron. The mentioned "optimized" biasing scheme is actually worse than the others. Finite boundaries are not included in our analysis, even though Sec. VII C illustrates that they can be important, because the needed information is not provided in the experimental account.

A choice was made to keep the center electrode and the plane outside the electrodes at the same potential. This is an added constraint, $\widetilde{V}_1 = 0$, upon the four scaled parameters that determine the behavior of a three-gap trap: $\widetilde{V}_1$, $\widetilde{V}_2$, $\widetilde{V}_3$, and $\tilde{z}_0$. Two additional constraints, $C_1 = 0$ and $C_2 = 1$, are required to form a trap. With the optional constraint there is one more parameter than there are constraints. If we choose $\tilde{z}_0$ as the corresponding free parameter, Fig. 20(a) shows the bias potentials that must be applied to realize each possible value of $\tilde{z}_0$. Figure 20(b) gives the corresponding a_k and C_k. For

TABLE XIII. Scaled parameters for the trap used in Ulm [13].

| | $\{\widetilde{\rho}_i\} = \{1, 3, 5\}$ [Eq. (C1)] | | | |
| | Used | | | Mentioned |
	Eq. (C2)	Eq. (C3)	Eq. (C4)	Eq. (C5)
$\widetilde{V}_1$	0	0	0	0
$\widetilde{V}_2$	−4.6075	−5.2815	−5.2040	22.3016
$\widetilde{V}_3$	−4.6075	−14.2194	−15.1782	−58.2296
$\widetilde{z}_0$	1.4761	1.9070	1.9493	3.9328
C_3	−0.6386	−0.4251	−0.4082	−0.3267
C_4	0.2718	0.1340	0.1211	0.0540
C_5	−0.0766	−0.0443	−0.0389	−0.0015
C_6	−0.0021	0.0141	0.0129	−0.0021
a_2	−0.1785	−0.0689	−0.0654	−0.0596
a_3	0.1140	0.0293	0.0267	0.0195
a_4	−0.0447	−0.0143	−0.0127	−0.0041
a_5	0.0088	0.0074	0.0065	0.0007
a_6	0.0026	−0.0030	−0.0026	−0.0001
C_{11}	−0.3529	−0.2003	−0.1902	−0.0299
C_{12}	−0.1287	−0.2004	−0.2029	−0.1188
C_{13}	0.1287	0.0744	0.0696	−0.0455
$C_{1d}^{(\text{opt})}$	−0.5215	−0.4037	−0.3949	−0.1957
$\tilde{\rho}_d^{(\text{opt})}$	2.0875	2.6969	2.7568	5.5618
γ_1	−4.89	0.47	0.07	30.26
γ_2	−5.27	−8.32	−10.05	−82.50
γ_3	−1.09	1.49	2.80	−194.34

TABLE XIV. Absolute values for the trap used in Ulm [13]. Axial frequencies calculated here differ from those reported in Ref. [13], which claims $f_z = 62.2$ MHz and 67.97 MHz for the potentials given in columns 1 and 2, respectively, of this table.

| | $\{\tilde{\rho}_i\} = \{1, 3, 5\}$ [Eq. (C1)] | | | | |
| | Used | | | Mentioned | |
	Eq. (C2)	Eq. (C3)	Eq. (C4)	Eq. (C5)	
ρ_1	1	1	1	1	mm
z_0	1.4761	1.9070	1.9493	3.9328	mm
$\rho_d^{(\text{opt})}$	2.0875	2.6969	2.7568	5.5618	mm
f_z	82.2714	66.2300	64.1039	14.1339	MHz
V_0	-1.5193	-0.9846	-0.9224	-0.0448	V
V_1	0	0	0	0	V
V_2	7	5.2	4.8	-1	V
V_3	7	14	14	2.611	V
Δf_z @ 5 K	8.3	4.0	3.9	16.2	kHz
Δf_z @ 300 K	500	240	235	971	kHz
$1 : \gamma_z$	2π 13.96	2π 4.50	2π 4.06	2π 0.10	s^{-1}
$2 : \gamma_z$	2π 1.86	2π 4.50	2π 4.61	2π 1.58	s^{-1}
$3 : \gamma_z$	2π 1.86	2π 0.62	2π 0.54	2π 0.23	s^{-1}
$d : \gamma_z^{(\text{opt})}$	2π 30.49	2π 18.27	2π 17.49	2π 4.30	s^{-1}

reasonable $\tilde{z}_0 \leqslant \tilde{\rho}_N$ we find that $|a_2| \geqslant 0.05$. Having explored what trap performance is possible with the optional constraint, we note that there is no compelling reason to make this choice. In fact such a choice would make it impossible to identify optimized planar Penning trap configurations.

It is possible to bias the Ulm trap electrodes to make $C_3 = 0$ by choosing $V_3/V_2 = -3.533$ for any $V_2 > 0$. However, this choice also results in $C_4 = -0.77$ and $a_2 = 0.58$, the latter
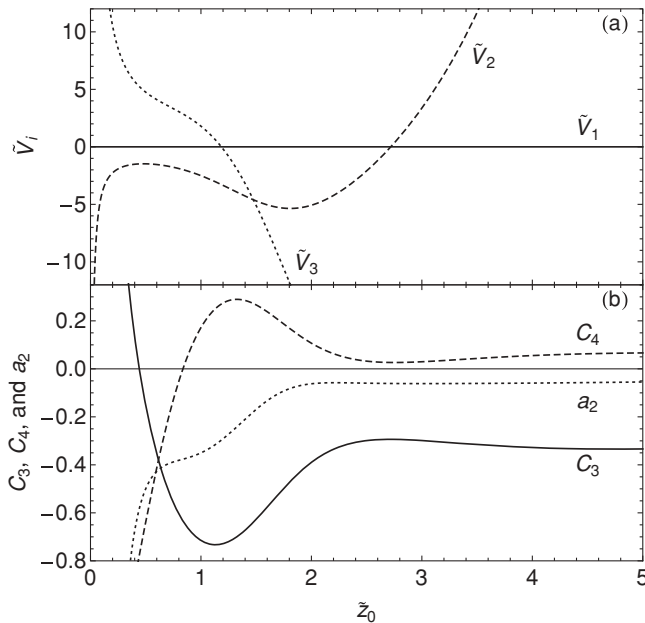

FIG. 20. (a) Scaled potentials applied to the Ulm trap to get a particular $\tilde{z}_0$. (b) Resulting trap properties for each $\tilde{z}_0$. The trap is biased subject to the optional constraint $V_1 = \tilde{V}_1 = 0$. It is not possible to make a_2 very small.

being worse than for the configurations in Table XIII. For this relative trap geometry, relaxing the optional constraint $V_1 = 0$ does not improve the trap performance.

Observing a single electron will be difficult if the thermal broadening of the axial frequency, Δf_z, is very large compared to the damping linewidth, $\gamma_z/(2\pi)$. Table XIV shows that this is indeed the case if the axial temperature is as low as 5 K, the lowest effective axial temperature that has been achieved without feedback cooling [29]. The heat generated in the detection amplifier makes it very difficult to achieve such a temperature, even for 0.1 K surroundings, so the effective axial temperature could easily have been much higher than 5 K. The table shows the thermal broadening for an effective axial temperature of 300 K.

Reference [13] says that a still broader width of 3 MHz "is expected and is in agreement with the measured data." Why this particular width should be expected is not specified. However, it is not surprising that the observed frequency width is larger than we calculate because the width grows with the large and unknown number of electrons in the trap. Experimental experience in our laboratory also suggests that it is likely that the observed width is broadened by charges accumulated on the insulator within the gaps since nothing in the circuit board technology used screens the potential from such charges.

One further item may be worth mentioning even though it is not completely understood. Many years ago, the first trap cooled with a dilution refrigerator was located on the still of the refrigerator, within the refrigerator's inner vacuum container (IVC). The vacuum was expected to be extremely good once the helium gas used to precool the IVC was pumped out. However, no good one-electron signals were ever observed, for reasons not clearly understood, but seemingly related to the cryopumped gas on the surface of the electrodes. Only when the trap vacuum was separated from the IVC vacuum did we get the clean signals used to resolve one-quantum transitions with one electron [1]. The Ulm trap was also located within the IVC vacuum. The long trapping lifetime observed with many trapped particles confirmed the expectation of a very good vacuum. Whether isolating the trap vacuum from the IVC would improve the observed signals has not been investigated at Ulm.

Is it possible to observe a single electron in a planar trap? Reference [13] concludes that it is not because the anharmonicity will always be too great, and it also reports that a thermal width narrower than 5 kHz could not be calculated for any N-gap trap where N is anything between 1 and 6. The only hope offered was that a much smaller trap might make the damping rate large enough to observe one electron despite the anharmonicity inherent in planar traps [13,14]. Indeed, Eq. (70) shows that when the trap dimension is decreased the damping rate increases as the square of dimension. With micro-fabrication methods it should be possible to fabricate smaller traps that thus will have a much larger damping. What remains to be demonstrated is that the anharmonicity will not become large enough for small traps to offset the damping advantage.

Our conclusion is different and much more optimistic. We agree that it should be very difficult to observe a single electron in the planar Penning trap used at Ulm. However, the fundamental problem is the relative geometry of the

Ulm trap, not its size. The thermal broadening is too great as a result of a choice of trap geometry that cannot be optimized to make $a_2 = 0$. Nonetheless, the conclusion [13] that it is "impossible" to observe a single electron in a planar Penning trap with a mm size scale now seems much too

strong. The optimized geometries and applied potentials that we present here for planar Penning traps of any size offer the possibility of a very large reduction in the critical amplitude dependence of the axial frequency. Experimental trials are warranted.

[1] S. Peil and G. Gabrielse, Phys. Rev. Lett. **83**, 1287 (1999).

[2] D. Hanneke, S. Fogwell, and G. Gabrielse, Phys. Rev. Lett. **100**, 120801 (2008).

[3] S. Mancini, A. M. Martins, and P. Tombesi, Phys. Rev. A **61**, 012303 (1999).

[4] G. Ciaramicoli, I. Marzoli, and P. Tombesi, Phys. Rev. A **63**, 052307 (2001).

[5] G. Ciaramicoli, I. Marzoli, and P. Tombesi, J. Mod. Opt. **49**, 1307 (2002).

[6] G. Ciaramicoli, I. Marzoli, and P. Tombesi, Phys. Rev. Lett. **91**, 017901 (2003).

[7] G. Ciaramicoli, I. Marzoli, and P. Tombesi, Phys. Rev. A **70**, 032301 (2004).

[8] G. Ciaramicoli, F. Galve, I. Marzoli, and P. Tombesi, Phys. Rev. A **72**, 042323 (2005).

[9] G. Ciaramicoli, I. Marzoli, and P. Tombesi, Int. J. Mod. Phys. B **20**, 1699 (2006).

[10] S. Stahl, F. Galve, J. Alonso, S. Djekic, W. Quint, T. Valenzuela, J. Verdú, M. Vogel, and G. Werth, Eur. Phys. J. D **32**, 139 (2005).

[11] F. Galve, P. Fernández, and G. Werth, Eur. Phys. J. D **40**, 201 (2006).

[12] F. Galve and G. Werth, Hyperfine Interact. **174**, 41 (2007).

[13] P. Bushev, S. Stahl, R. Natali, G. Marx, E. Stachowska, G. Werth, M. Hellwig, and F. Schmidt-Kaler, Eur. Phys. J. D **50**, 97 (2008); **57**, 301 (2010).

[14] I. Marzoli, P. Tombesi, G. Ciaramicoli, G. Werth, P. Bushev, S. Stahl, F. Schmidt-Kaler, M. Hellwig, C. Henkel, G. Marx, I. Jex, E. Stachowska, G. Szawiola, and A. Walaszyk, J. Phys. B **42**, 154010 (2009).

[15] D. Cruz, J. P. Chang, M. Fico, A. J. Guymon, D. E. Austin, and M. G. Blain, Rev. Sci. Instrum. **78**, 015107 (2007).

[16] G. Gabrielse and F. C. MacKintosh, Int. J. Mass Spectrom. Ion Processes **57**, 1 (1984).

[17] G. Gabrielse, Phys. Rev. A **27**, 2277 (1983).

[18] G. Gabrielse, Phys. Rev. A **29**, 462 (1984).

[19] S. Rainville, J. K. Thompson, and D. E. Pritchard, Science **303**, 334 (2004).

[20] G. Gabrielse, L. Haarsma, and S. L. Rolston, Int. J. Mass Spectrom. Ion Processes **88**, 319 (1989); **93**, 121 (1989).

[21] G. Gabrielse, A. Khabbaz, D. S. Hall, C. Heimann, H. Kalinowsky, and W. Jhe, Phys. Rev. Lett. **82**, 3198 (1999).

[22] H. Häffner, T. Beier, N. Hermanspahn, H.-J. Kluge, W. Quint, S. Stahl, J. Verdú, and G. Werth, Phys. Rev. Lett. **85**, 5308 (2000).

[23] J. Verdú, S. Djekić, S. Stahl, T. Valenzuela, M. Vogel, G. Werth, T. Beier, H.-J. Kluge, and W. Quint, Phys. Rev. Lett. **92**, 093002 (2004).

[24] G. Werth, J. Alonso, T. Beier, K. Blaum, S. Djekic, H. Häffner, N. Hermanspahn, W. Quint, S. Stahl, J. Verdú, T. Valenzuela, and M. Vogel, Int. J. Mass Spectrom. **251**, 152 (2006).

[25] J. D. Jackson, *Classical Electrodynamics*, 3rd ed. (Wiley, New York, 1999).

[26] B. Kusse and E. Westwig, *Mathematical Physics: Applied Mathematics for Scientists and Engineers* (Wiley, New York, 1998).

[27] L. D. Landau and E. M. Lifshitz, *Mechanics (Third Edition)* (Pergamon Press, New York, 1976).

[28] R. E. Mickens, *An Introduction to Nonlinear Oscillations* (Cambridge University Press, Cambridge, England, 1981).

[29] B. D'Urso, B. Odom, and G. Gabrielse, Phys. Rev. Lett. **90**, 043001 (2003).

[30] J. N. Tan and G. Gabrielse, Appl. Phys. Lett. **55**, 2144 (1989).

[31] L. S. Brown and G. Gabrielse, Rev. Mod. Phys. **58**, 233 (1986).

[32] B. D'Urso, R. Van Handel, B. Odom, D. Hanneke, and G. Gabrielse, Phys. Rev. Lett. **94**, 113002 (2005).

[33] R. J. Noer, Appl. Phys. A **28**, 1 (1982).

[34] C. Suzuki, T. Nakanishi, S. Okumi, T. Gotou, K. Togawa, F. Furuta, K. Wada, T. Nishitani, M. Yamamoto, J. Watanabe, S. Kurahashi, K. Asano, H. Matsumoto, M. Yoshioka, and H. Kobayakawa, Nucl. Instrum. Methods Phys. Res. A **462**, 337 (2001).

[35] F. Le Pimpec, R. Ganter, and R. Betemps, Nucl. Instrum. Methods Phys. Res. A **574**, 7 (2007).

[36] D. Cruz, J. P. Chang, and M. G. Blain, Appl. Phys. Lett. **86**, 153502 (2005).

[37] M. Hellwig, A. Bautista-Salvador, K. Singer, G. Werth, and F. Schmidt-Kaler, e-print arXiv:0912.1533v3 (2010).

[38] F. H. L. Koppens, C. Buizert, K. J. Tielrooij, I. T. Vink, K. C. Nowack, T. Meunier, L. P. Kouwenhoven, and L. M. K. Vandersypen, Nature (London) **442**, 766 (2006).

[39] D. Wineland, P. Ekstrom, and H. Dehmelt, Phys. Rev. Lett. **31**, 1279 (1973).